SUPPORTING INFORMATION

Switchable Solid-State Emission in GFP Chromophore Analogue Cocrystals via Competing AIE and ACQ Pathways

Bhupendra P. Mali,[ab†] Niteen B. Dabke,[ab†] Himanshu Sharma,[ab] Soumya Ranjan Dash,[ab]

Kochunnoonny Manoj,[c] Kumar Vanka,[ab] Rajesh G. Gonnade[ab*]*

[a]*Physical and Materials Chemistry Division, CSIR-National Chemical Laboratory,*

Dr. Homi Bhabha Road, Pashan, Pune 411008, India.

[b]*Academy of Scientific and Innovative Research (AcSIR), Ghaziabad 201002, India.*

[c]*Institution Research and Development Laboratory, Alchemy Innovative Solutions Kochi, Kerala 683544, India.*

Correspondence email: rg.gonnade.ncl@csir.res.in; *k.vanka.ncl@csir.res.in*

† These authors contributed equally.

Contents

Experimental Section:

1. Materials:

The reagents and starting materials for synthesis were purchased from Sigma-Aldrich and TCI Chemicals, and all HPLC-grade solvents were obtained from Finar and used without further purification.

2. Coformers:

Perfluoronaphthalene (A), benzene-1,2,4,5-tetracarbonitrile (B), and 2,3,4,5,6-pentafluorophenol (C) were purchased from Sigma Aldrich and used without further purification.

3. Single Crystal X-Ray Diffraction Studies:

Good-quality single crystals of each cocrystal, suitable for single-crystal X-ray diffraction analysis, were selected using a Leica polarizing microscope (S8 APO). The X-ray intensity data for each cocrystal were measured on a Bruker D8 VENTURE Kappa Duo PHOTON II CPAD diffractometer equipped with Incoatech multilayer mirror optics, with an X-ray generator power setting of 50 kV and 1.4 mA. The intensity measurements were carried out with a Mo microfocus sealed tube diffraction source (MoKα = 0.71073 Å) at 100(2) K for all cocrystals. A preliminary set of cell constants and an orientation matrix were calculated from a total of 36 frames (matrix, three runs, each run comprised of 12 frames). The full-intensity data were collected using an optimized strategy that consisted of different sets of ω, φ and 2θ with a 0.5° width, keeping the sample-to-detector distance fixed at 5.00 cm and varying the exposure time (10-20 sec) depending on the diffraction power of the crystals. The whole process of X-ray data acquisition (unit–cell measurements and data collection) was controlled and monitored by the APEX3 program suite of Bruker-AXS.[1] The complete data sets were corrected for Lorentz-polarization and absorption effects (multi-scan method) by using SAINT and SADABS programs with the transmission coefficients. Using the APEX3[1] program suite, the structure was solved with the ShelXS-97[2] structure solution program, employing direct

methods. The model was refined using a version of ShelXL-2013[3] with least squares minimization based on F^2. All non-hydrogen atoms were refined anisotropically, whereas hydrogen atoms were refined isotropically by placing them in geometrically idealized positions. The molecular packing diagrams were generated using the Mercury program.[4] Geometrical calculations were performed using SHELXTL[1] and PLATON.[5] Experiment details of the single-crystal X-ray diffraction analysis, including crystal data, data collection, and structure refinement for all the cocrystals, are summarized in Table S2.

4. Hirshfeld Surface Analysis:

Hirshfeld surface analysis was performed using *CrystalExplorer* (v. 17.5)[6] to determine the percentage contributions of intermolecular interactions. Hirshfeld surfaces[7] and corresponding fingerprint plots[8] were generated to compare these interactions. Lattice energy calculations were performed using *CrystalExplorer* to obtain quantitative insights into the magnitudes of donor-acceptor pair interactions. A cluster of molecules was generated within a 3.8 Å radius to evaluate intermolecular interactions and pairwise interaction energies.[9] The total interaction energy (E_{tot}) was estimated after taking into account the electrostatic (E_{ele}), polarization (E_{pol}), dispersion (E_{dis}), and exchange-repulsion (E_{rep}) energy contributions. The calculations were performed based on their crystal geometries using the B3LYP hybrid functional and the 6-311++G(d,p) basis sets.

5. Powder X-Ray Diffraction Studies:

The D8 VENTURE single-crystal X-ray diffractometer from Bruker was used for the experimental PXRD studies. The intensity measurements were carried out using a Cu micro-focus sealed tube diffraction source (Cu Kα = 1.54178 Å) at a temperature of 100(2) K, as well as at specified temperatures for variable temperature PXRD. The sample was rotated to complete a 360-degree rotation with uniform speed and exposed for 120 seconds for all scans. After completing all scans, the Debye rings were integrated to create a raw file, which was then

converted to an xrdml file using *PowDLL Converter*.[10] PXRD graphs with background correction was then plotted.

6. Thermal Studies:

Differential scanning calorimetry (DSC) was conducted using a Mettler Toledo DSC 822e instrument to measure the enthalpy change. The crystals of all the cocrystals were first air-dried to remove the traces of the solvent from the crystal surface. Dried crystals were taken on an aluminum pan (40 μL) and crimped. The pan was heated from room temperature (298 K) to 473 K at a rate of 10 K min^{-1} using an empty aluminum pan as a reference. Dry nitrogen gas was used for purging. Furthermore, thermogravimetric analysis (TGA) was performed using SDT Q600 instrument at heating rate of 10°C/min under nitrogen atmosphere.

7. TD-DFT Studies:

TD-DFT calculations were performed at the B3LYP/6-311++G(d,p)[11] level of theory. The calculated values of the UV-Vis transition corresponding to the first excitation state, which involves the HOMO and the LUMO orbitals, were in close agreement with the experimental values (Table S10). Electrostatic potential (ESP) analysis and noncovalent interaction (NCI) plots were carried out using the Multiwfn[12] program and visualized in VMD.[13] Natural bond orbital (NBO) analysis was performed at the ωB97X-D/def2-TZVP[14,15] level to examine the charge transfer between the analogue and the coformer molecule.

8. Photophysical Measurements:

Absorption spectra were determined using a LAB INDIA UV-VIS spectrophotometer (model UV 3092) with an auto cell changer and high-intensity Tungsten, Halogen, and Deuterium lamp. PL decay dynamics were recorded using a fluorescence spectrometer (Edinburgh Instruments, Model FS5 spectrofluorometer) with a microsecond flash lamp of 100 W power. For photoluminescence decay dynamics, the sample was excited at 390 nm, using a

microsecond flash lamp. The relative quantum yield measurement was carried out using a fluorescence spectrometer (Edinburgh Instruments, Model FS5 spectrofluorometer).

Table S1. Crystallization of all the cocrystals of **1** from various common organic solvents by the slow evaporation method.

Cocrystals	**Solvents used for crystallization**
Cocrystal-**I** (**1**:A)	Methanol, Ethanol, Isopropyl alcohol, Dichloromethane, Chloroform, Ethyl acetate, Acetonitrile
Cocrystal-**II** (**1**:B)	Methanol, Ethanol, Isopropyl alcohol, Dichloromethane, Chloroform, Ethyl acetate, Acetonitrile
Cocrystal-**III** (**1**:C)	Methanol, Ethanol, Isopropyl alcohol, Dichloromethane, Chloroform,

Table S2. Crystallographic data for the cocrystals of **1**.

Crystal Data	Cocrystal-I	Cocrystal-IA	Cocrystal-II	Cocrystal-III
Formula	$C_{23}H_{20}N_2O_3 \cdot C_{10}F_8$	$C_{23}H_{20}N_2O_3 \cdot C_{10}F_8$	$2(C_{23}H_{20}N_2O_3) \cdot 2(C_{10}H_2N_4)$	$C_{23}H_{20}N_2O_3 \cdot C_6HF_5O$
M_r	644.51	644.51	1101.13	556.48
Crystal Size, mm	0.160 × 0.140 × 0.090	0.157 × 0.144 × 0.084	0.100 × 0.090 × 0.080	0.120 × 0.110 × 0.080
Temp. (K)	100(2)	348(2)	100(2)	100(2)
Crystal Syst.	Triclinic	Triclinic	Triclinic	Monoclinic
Space Group	$P\bar{1}$	$P\bar{1}$	$P\bar{1}$	$P2_1/c$
a/Å	7.5076(6)	7.660(2)	7.8420(3)	7.7363(3)
b/Å	11.7226(10)	11.953(4)	8.0067(3)	21.8852(8)
c/Å	15.5802(13)	15.946(5)	44.0828(19)	14.6478(6)
$\alpha^{/0}$	86.106(4)	93.457(7)	87.523(2)	90
$\beta^{/0}$	85.031(3)	92.705(7)	88.221(2)	93.0860(10)
$\gamma^{/0}$	86.792(3)	92.751(8)	78.9690(10)	90
V/Å^3	1361.2(2)	1453.8(8)	2713.48(19)	2476.43(17)
Z	2	2	4	4
D_{calc}/g cm^{-3}	1.573	1.472	1.348	1.493
m/mm^{-1}	0.138	0.129	0.090	0.125
F(000)	656	656	1144	1144
Ab. Correct.	multi-scan	multi-scan	multi-scan	multi-scan
T_{min}/ T_{max}	0.978/0.988	0.980/0.989	0.7034/0.7454	0.985/0.990
$2\theta_{max}$	50	50	50	50
Total reflns.	96813	14850	76978	68822
Unique reflns.	6294	5934	11065	6425
Obs. reflns.	5484	2027	9307	4996
h, k, l (min, max)	(-9,9), (-15, 15), (-20, 20)	(-9,8), (-14, 14), (-19, 19)	(-9, 9), (-9, 9), (-55, 55)	(-9, 10), (-29, 29), (-19, 19)
R_{int}	0.0686	0.1358	0.0571	0.0900
No. of para	417	422	761	365
R1 [$I > 2\sigma(I)$]	0.0531	0.1878	0.0537	0.0734
wR2[$I > 2\sigma(I)$]	0.1204	0.4600	0.1187	0.1318
R1 [all data]	0.0615	0.3358	0.0656	0.0997
wR2 [all data]	0.1243	0.5402	0.1240	0.1416
Goodness of fit	1.122	1.393	1.105	1.148
$\Delta\rho_{max}$, $\Delta\rho_{min}$ (eÅ^{-3})	+ 0.367, -0.290	+0.714, -0.675	+ 0.350, -0.351	+ 0.357, - 0.297
CCDC no.	2490012	not deposited	2490013	2490014

Table S3. The geometrical parameters of intermolecular interactions in cocrystals of **1**.

Entry	D-H···A	D-H (Å)	H···A (Å)	D···A (Å)	D-H···A	Symmetry Codes
Cocrystal-I						
1.	C19A-H19B···O1A	0.98	2.58	3.326(2)	133	*x*+1, *y*, *z*
2.	C19A-H19C···F6B	0.98	2.58	3.311(2)	131	*x*+1, *y*+1, *z*
3.	C23A-H23A···F3B	0.98	2.59	3.266(3)	126	-*x*+1, -*y*+1, -*z*+2
4.	C1B-F1B···Cg4	-	3.7162(14)	3.4965(18)	70	1-*x*, 1-*y*,1-*z*
5.	C1B -F1B···Cg5	-	3.6027(14)	3.3014(17)	66	-*x*, 1-*y*, 1-*z*
6.	C1B-F1B···Cg6	-	3.7190(13)	3.5733(16)	73	1-*x*, 1-*y*, 1-*z*
7.	C2B-F2B…Cg2	-	3.4319(15)	3.707(2)	91	1-*x*, 1-*y*, 1-*z*
8.	C2B-F2B···Cg3	-	3.4836(15)	3.369(2)	74	-*x*, 1-*y*, 1-*z*
9.	C2B-F2B···Cg5	-	3.5897(14)	4.227(2)	109	1-*x*, 1-*y*, 1-*z*
10.	C2B-F2B···Cg6	-	3.7347(14)	3.586(2)	73	1-*x*, 1-*y*, 1-*z*
11.	C2B-F2B···Cg7	-	3.4596(14)	3.729(2)	91	1-*x*, 1-*y*, 1-*z*
12.	C8B-F7B···Cg4	-	3.6908(15)	3.351(2)	65	-*x*, 1-*y*, 1-*z*
Cocrystal-II						
1.	C1B-H1B···N1A	0.95	2.35	3.198(3)	148	*x*, *y*, *z*
2.	C1D-H1D···N1C	0.95	2.34	3.203(2)	150	*x*, *y*, *z*
3.	C4B-H4B···N2B	0.99	2.47	3.342(2)	153	*2*-*x*, 2-*y*, 1-*z*
4.	C4D-H4D···N2D	0.95	2.45	3.339(2)	155	-*x*, 1-*y*, 2-*z*
5.	C13A-H13A···N3B	0.99	2.49	3.286(3)	141	-*1*+*x*, -1+*y*, *z*
6.	C13C-H13C···N3D	0.95	2.47	3.267(3)	141	*1*+*x*, 1+*y*, *z*
7.	C20A-H20A···O3C	0.99	2.59	3.579(2)	176	*x*, -1+*y*, *z*
8.	C20A-H20B···O2C	0.99	2.44	3.184(2)	131	*x*, *y*, *z*
9.	C4A -H4A···Cg1	-	2.87	3.552(2)	129	*1*+*x*, *y*, *z*
10.	C4C -H4C···Cg8	-	2.91	3.519(2)	123	*x*, -1+*y*, *z*
11.	C5C -H5C···Cg8	-	2.90	3.504(3)	123	*x*, -1+*y*, *z*
Cocrystal-III						
1.	O1B-H1B···N1A	0.84	1.86	2.67(2)	160	*x*+1, *y*, *z*

2.	C20A-H20A···F3B	0.99	2.51	3.18(3)	125	*x*-1/2, -*y*+1/2, *z*-1/2
3.	C22A-H22A···O2A	0.99	2.63	3.450(3)	141	-*x*+1, -*y*+1, -*z*+1
4.	C19A-H19C···O2A	0.98	2.61	3.278(3)	125	*x*, *y*, *z*
5.	C23A-H23C···Cg4	-	2.93	3.740(3)	140	1/2-*x*, 1/2+*y*, 1/2-*z*
6.	C2B-F1B···Cg2	-	3.9806(18)	4.102(3)	86	1+*x*, *y*, *z*
7.	C2B-F1B···Cg4	-	3.2573(18)	3.649(3)	96	*x*, *y*, *z*
8.	C2B-F1B···Cg6	-	3.5047(17)	3.442(2)	76	*x*, 1+*y*, *z*
9.	C3B-F2B···Cg2	-	3.6077(18)	3.368(3)	69	*x*, *y*, *z*
10.	C3B-F2B···Cg6	-	3.5957(18)	3.485(3)	74	*x*, *y*, *z*
11.	C3B-F2B···Cg7	-	3.5572(17)	3.321(2)	69	*x*, *y*, *z*
12.	C4B-F3B···Cg3	-	3.4897(19)	3.655(3)	86	*x*, *y*, *z*
13.	C4B-F3B···Cg5	-	3.5990(18)	3.429(3)	72	*x*, *y*, *z*
14.	C5B-F4B···Cg1	-	3.1212(18)	4.192(3)	136	1/2+*x*, 1/2-*y*, 1/2+*z*
15.	C6B-F5B···Cg3	-	3.8586(18)	3.474(3)	64	1+*x*, *y*, *z*

D-H = Donor- Hydrogen bond length in Angstrom (Å), H···A = Hydrogen···Acceptor bond length in Angstrom (Å), D···A = Donor···Acceptor bond length in Angstrom (Å), D-H···A = bond angle in degrees (°), For

Cocrystal-I: *Cg*1: N1A/C17A/C16A/N2A/C18A; *Cg*2: C1A/C2A/C7A/C8A/C9A/C14A; *Cg*3: C2A-C7A; *Cg*4: C9A-C14A; *Cg*5: C1A-C9A/C14A; *Cg*6: C1A/C2A/C7A-C14A; *Cg*7: C1A-C14A; *Cg*8: C1B-C5B/C10B; *Cg*9: C5B-C10B; *Cg*10: C1B-C10B.

Cocrystal-II: *Cg*1: N1A/C16A/C17A/N2A/C18A; *Cg*2: C1A/C2A/C7A/C8A/C9A/C14A; *Cg*3: C2A-C7A; *Cg*4: C9A-C14A; *Cg*5: C1A-C9A/C14A; *Cg*6: C1A/C2A/C7A-C14A; *Cg*7: C1A-C14A; *Cg*8: N1C/C16C/C17C/N2C/C18C; *Cg*9: C1C/C2C/C7C/C8C/C9C/C14C; *Cg*10: C2C-C7C; *Cg*11: C9C-C14C; *Cg*12: C1C-C9C/C14C; *Cg*13: C1C/C2C/C7C-C14C; *Cg*14: C1C-C14C; *Cg*15: C1B-C6B; *Cg*16: C1D-C6D.

Cocrystal-III: *Cg*1: N1A/C16A/C17A/N2A/C18A; *Cg*2: C1A/C2A/C7A/C8A/C9A/C14A; *Cg*3: C2A-C7A; *Cg*4: C9A-C14A; *Cg*5: C1A-C9A/C14A; *Cg*6: C1A/C2A/C7A-C14A; *Cg*7: C1A-C14A; *Cg*8: C1B-C6B.

Table S4. The geometrical parameters of π···π interactions in cocrystals of **1**.

Entry	D-H···A	Cg···Cg (Å)	α (°)	CgI-Perp	CgJ-Perp	Slippage	Symmetry Codes
Cocrystal-I							
1	Cg1···Cg1	3.5095(11)	0.02(10)	3.2992(7)	3.2992(7)	1.197	1-*x*, 1-*y*, 1-*z*
2	Cg2···Cg8	3.6856(11)	5.42(8)	3.3108(6)	3.4234(8)	1.365	-*x*, 1-*y*, 1-*z*
3	Cg2···Cg9	3.7656(11)	3.53(8)	3.3409(6)	3.4115(7)	1.594	-*x*, 1-*y*, 1-*z*
4	Cg2···Cg10	3.5235(9)	4.40(6)	3.3474(6)	3.4207(6)	0.845	-*x*, 1-*y*, 1-*z*
5	Cg3···Cg8	3.8076(12)	5.40(9)	3.2986(8)	3.4230(8)	1.668	-*x*, 1-*y*, 1-*z*
6	Cg4···Cg8	3.7907(11)	7.40(8)	3.4765(6)	3.2588(8)	1.936	1-*x*, 1-*y*, 1-*z*
7	Cg4···Cg9	3.5664(10)	5.10(8)	3.3328(6)	3.4093(7)	1.047	-*x*, 1-*y*, 1-*z*
8	Cg4···Cg10	3.8735(9)	6.24(6)	3.4448(6)	3.3065(6)	2.018	1-*x*, 1-*y*, 1-*z*
9	Cg5···Cg8	3.5382(10)	5.33(7)	3.3028(6)	3.4056(8)	0.959	-*x*, 1-*y*, 1-*z*
10	Cg5...Cg10	3.7856(9)	4.43(5)	3.3244(6)	3.4194(6)	1.624	-*x*, 1-*y*, 1-*z*
11	Cg6···Cg8	3.9256(10)	6.44(7)	3.4465(5)	3.2892(8)	2.143	-*x*, 1-*y*, 1-*z*
12	Cg6···Cg9	3.4517(9)	4.25(7)	3.3334(5)	3.3866(7)	0.667	-*x*, 1-*y*, 1-*z*
13	Cg6···Cg10	3.6220(8)	5.31(5)	3.3248(5)	3.4213(6)	1.189	-*x*, 1-*y*, 1-*z*
14	Cg7···Cg8	3.6463(10)	5.94(7)	3.2787(5)	3.4000(8)	1.317	-*x*, 1-*y*, 1-*z*
15	Cg7···Cg9	3.7291(10)	3.98(6)	3.3078(5)	3.3772(7)	1.581	-*x*, 1-*y*, 1-*z*
16	Cg7···Cg10	3.4835(8)	4.90(5)	3.3148(5)	3.3918(6)	0.794	-*x*, 1-*y*, 1-*z*
Cocrystal-II							
1	Cg2···Cg15	3.8894(10)	3.61(8)	3.4842(7)	3.4199(7)	1.853	-1+*x*, *y*, *z*
2	Cg3···Cg15	3.5179(11)	2.66(9)	3.3356(9)	3.3484(7)	1.079	*x*, *y*, *z*
3	Cg4···Cg15	3.6339(11)	2.86(9)	3.3556(8)	3.4168(7)	1.238	-1+*x*, *y*, *z*
4	Cg5···Cg15	3.6382(9)	2.99(7)	3.3983(6)	3.3651(7)	1.383	*x*, *y*, *z*
5	Cg6···Cg15	3.5612(9)	3.27(7)	3.4217(6)	3.4272(7)	0.968	-1+*x*, *y*, *z*
6	Cg7···Cg15	3.8931(9)	3.01(6)	3.4828(6)	3.4179(7)	1.864	-1+*x*, *y*, *z*
7	Cg9···Cg16	3.7752(9)	2.17(8)	3.4064(7)	3.3693(7)	1.703	1+*x*, *y*, *z*
8	Cg10···Cg16	3.5078(11)	2.37(9)	3.3334(9)	3.3390(7)	1.075	*x*, *y*, z
9	Cg11···Cg16	3.6057(11)	1.29(9)	3.3426(9)	3.3721(7)	1.277	1+*x*, *y*, *z*

10	Cg12···Cg16	3.6037(9)	2.10(7)	3.3767(6)	3.3489(7)	1.33	*x*, *y*, z
11	Cg13···Cg16	3.4848(9)	1.73(7)	3.3768(6)	3.3837(7)	0.833	1+*x*, *y*, *z*
Cocrystal-III							
1	Cg2···Cg8	3.6619(14)	5.61(11)	3.3671(9)	3.4689(10)	1.173	*x*, *y*, *z*
2	Cg3···Cg8	3.6115(14)	1.87(11)	3.3953(10)	3.4283(10)	1.135	-1+*x*, *y*, *z*
3	Cg4···Cg8	4.4447(14)	7.76(11)	3.1615(10)	3.5254(10)	2.707	*x*, *y*, *z*
4	Cg5···Cg8	3.9792(12)	3.56(9)	3.4474(7)	3.4377(10)	2.004	-1+*x*, *y*, *z*
5	Cg5···Cg8	3.7911(12)	3.56(9)	3.4053(7)	3.4344(10)	1.606	*x*, *y*, *z*
6	Cg6···Cg8	3.8830(12)	6.75(9)	3.2628(7)	3.4872(10)	1.708	*x*, *y*, *z*
7	Cg7···Cg8	3.6259(12)	5.11(9)	3.3199(6)	3.4217(10)	1.199	*x*, *y*, *z*

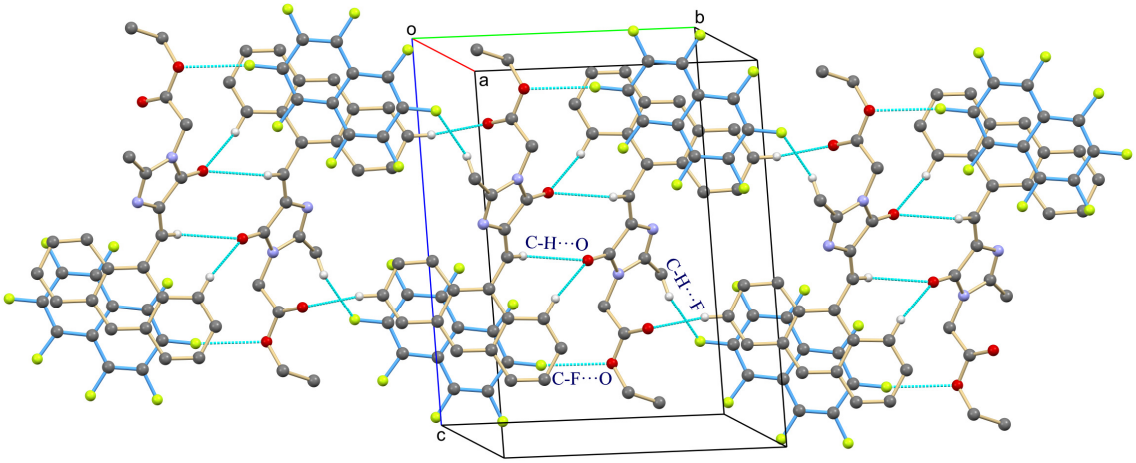

Figure S1. Molecular packing in the Cocrystal-**I**, showing formation of 1D molecular string parallel to the *b*-axis using C-H···O, C-H···F, and C-F···O interactions.

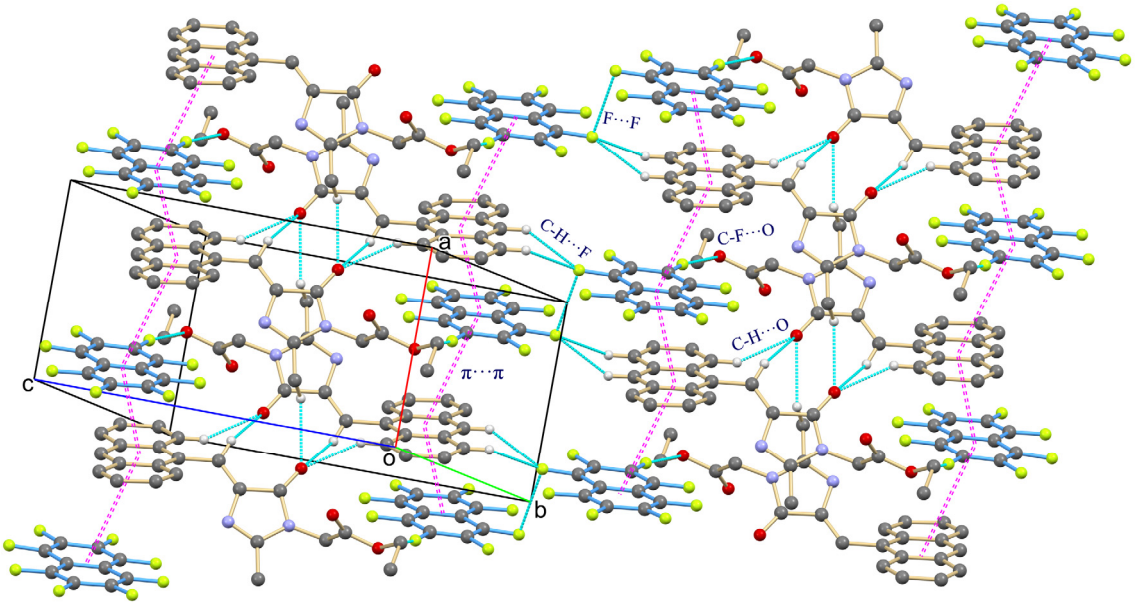

Figure S2. View of molecular packing in the Cocrystal-**I**, forming a columnar arrangement parallel to the *a*-axis, stabilized by C-H···O, C-H···F, C-F···O, F···F, and π···π interactions.

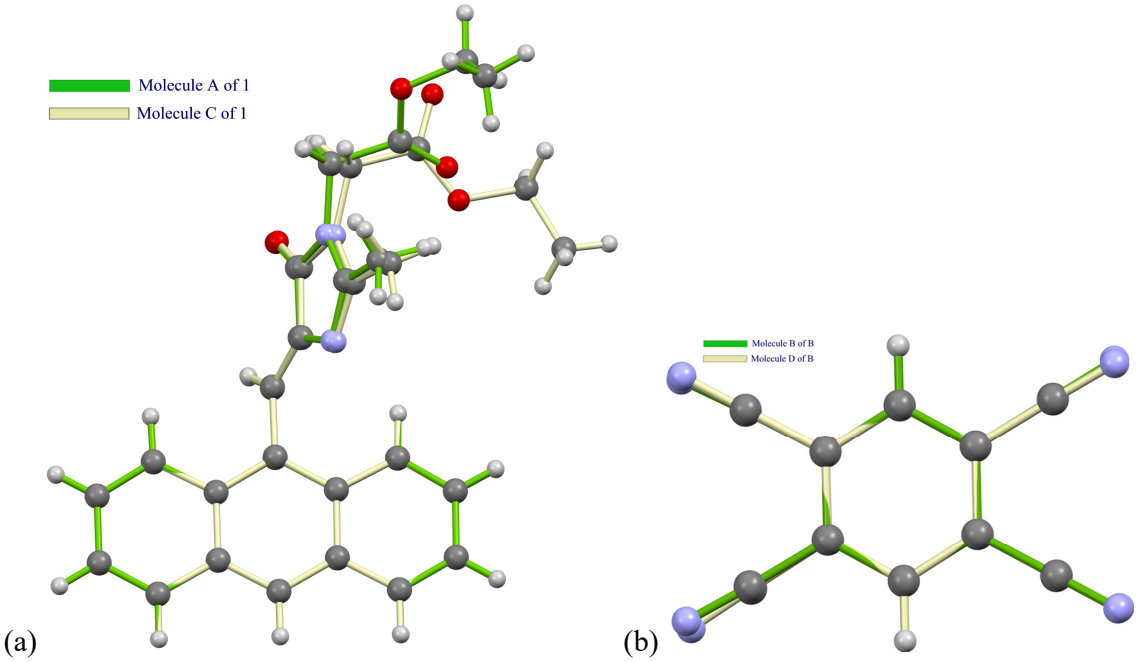

Figure S3. Overlay of the crystal structures of conformers of (a) **1** and (b) benzene-1,2,4,5-tetracarbonitrile in Cocrystal-**II**.

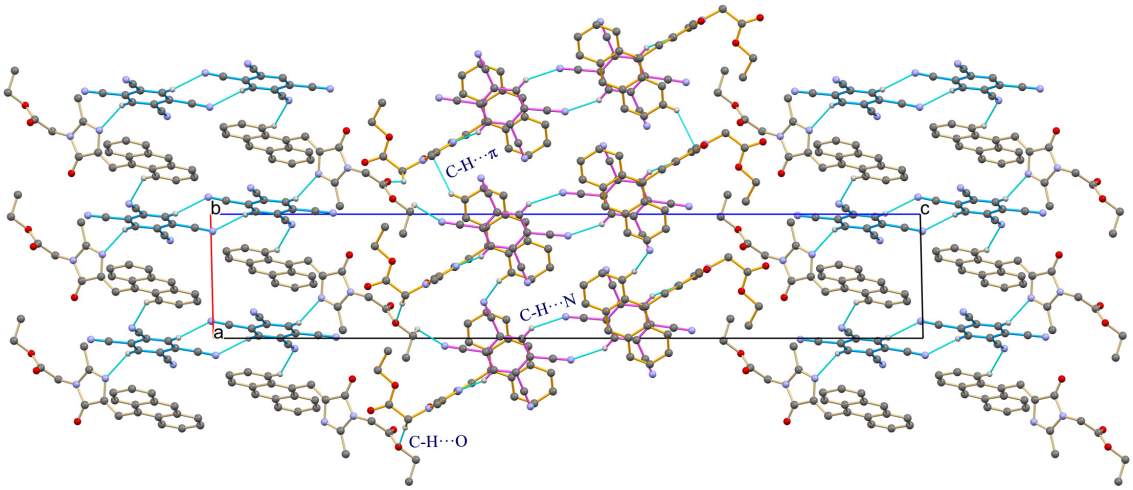

Figure S4. Molecular packing in Cocrystal-**II**, showing a close view of the joining of 1D molecular strings along the *c*-axis using C-H···O, C-H···N, C-H···π and π···π contacts.

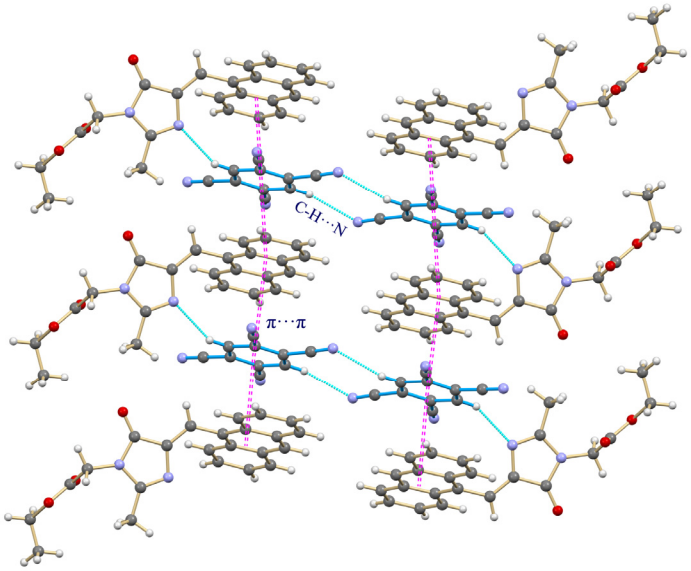

Figure S5. View of molecular packing in the Cocrystal-**II**, forming a columnar arrangement parallel to the *a*-axis, stabilized by C-H···N, and π···π interactions.

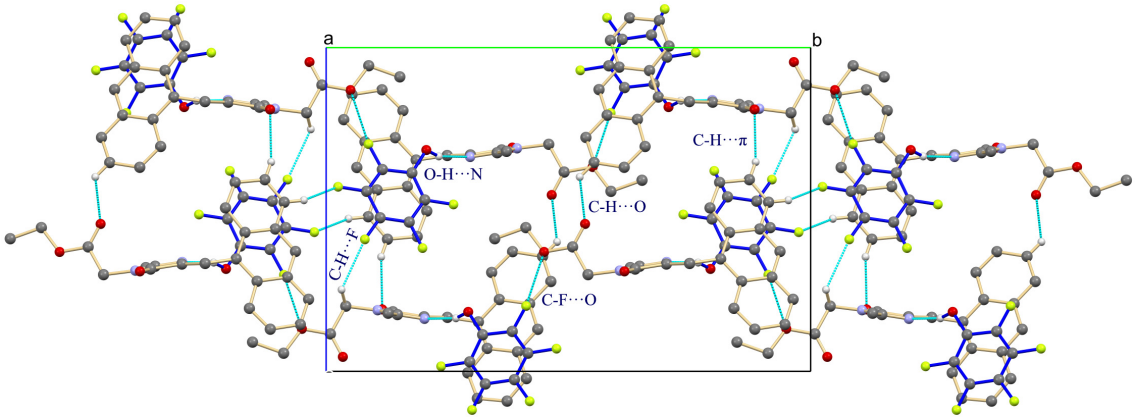

Figure S6. Molecular packing in the Cocrystal-**III**, showing formation of helical assembly parallel to the *b*-axis using C-H···O, C-H···F, C-F···O, C-H···π and π···π interactions.

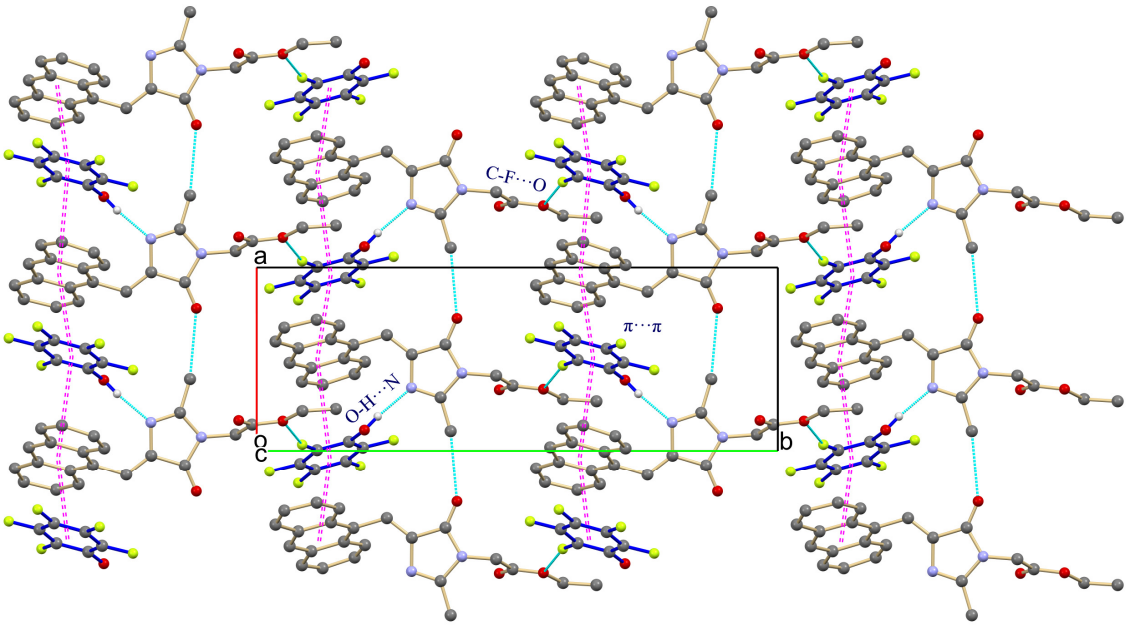

Figure S7. View of molecular packing in the Cocrystal-**III**, forming a columnar arrangement parallel to the *a*-axis, stabilized by O-H···N, C-F···O, and π···π interactions.

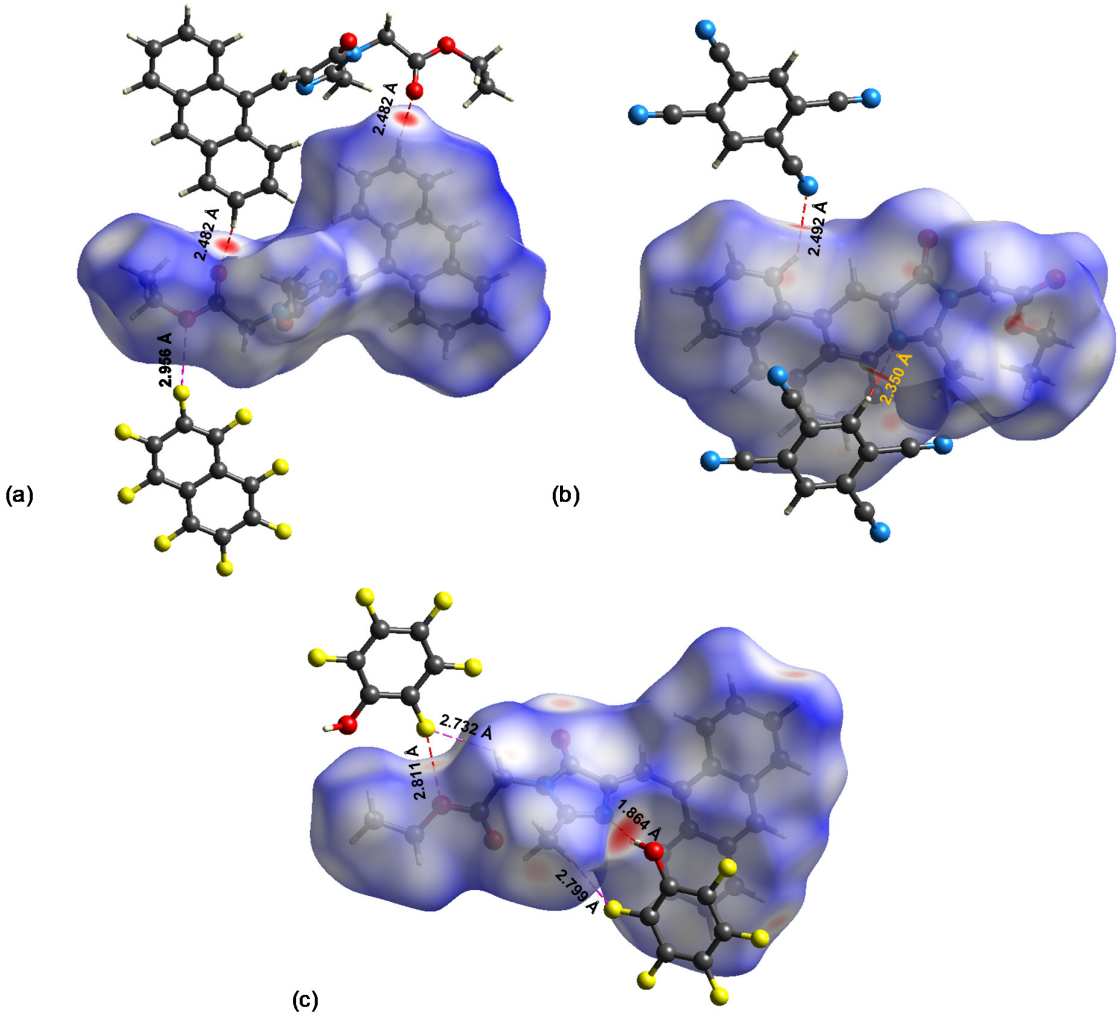

Figure S8. Hirshfeld surfaces plots for, (a) Cocrystal-**I**, (b) Cocrystal-**II** and (c) Cocrystal-**III**.

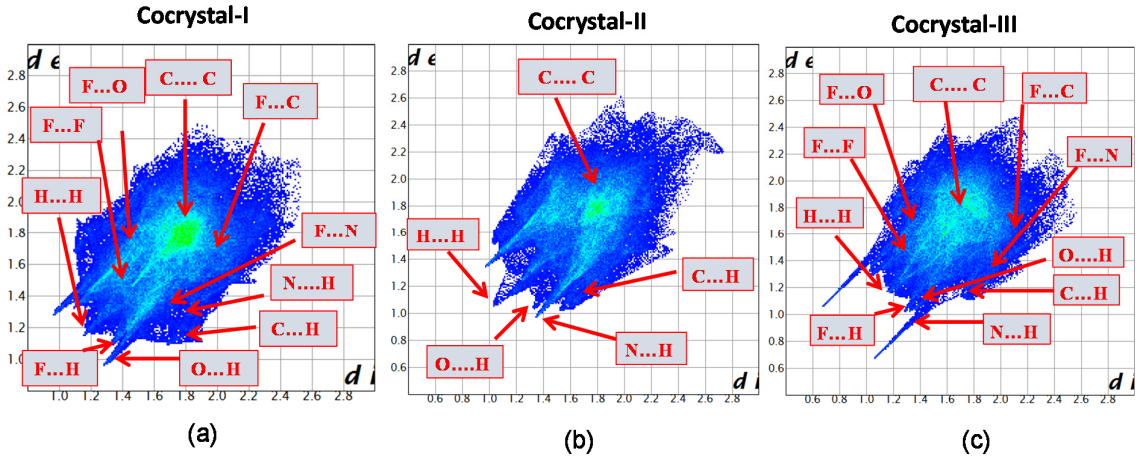

Figure S9. Fingerprint plots of the Hirshfeld surfaces for, (a) Cocrystal-**I**, (b) Cocrystal-**II** and (c) Cocrystal-**III**.

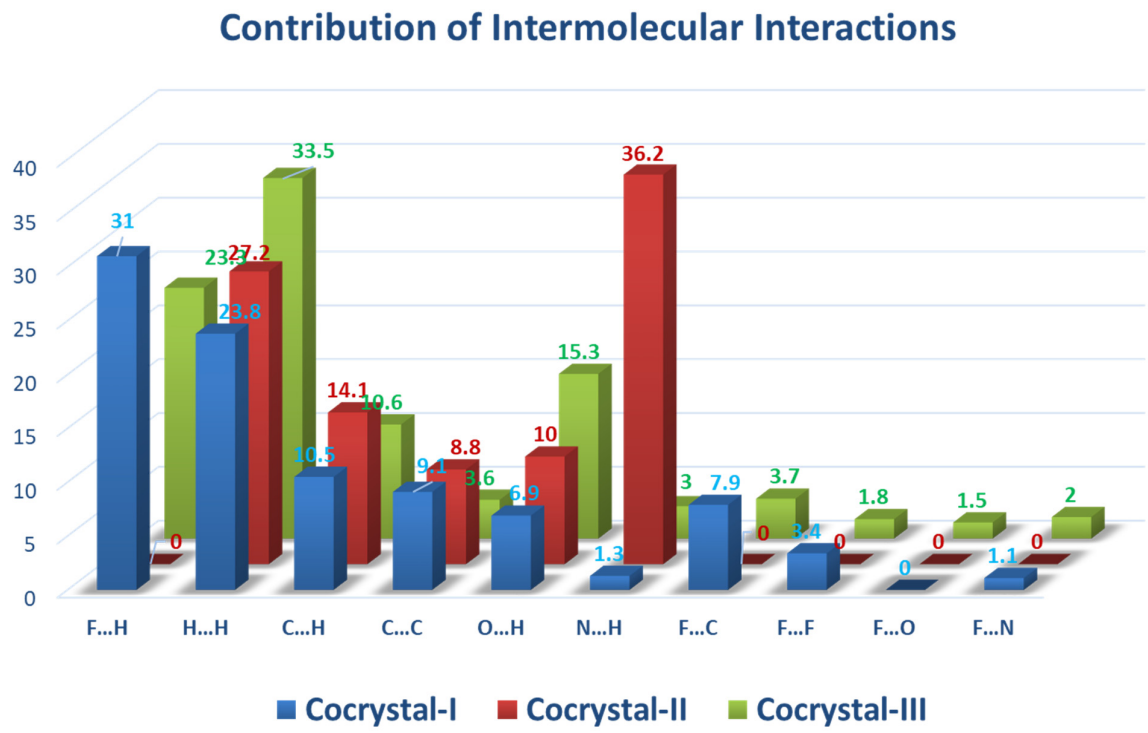

Figure S10. Percentage contribution of various intermolecular interactions to Hirshfeld surface areas in all the cocrystals of **1**.

Hirshfeld surface and 2D fingerprint analyses of the analogue and its cocrystals revealed an increase in C···C contacts, from 1.1% in the precursor analogue **1** (for Form **I** polymorph) to 9.1%, 8.8%, and 3.6% in Cocrystals **I, II**, and **III**, respectively, indicating the presence of strong π–π stacking interactions in the cocrystals. In Cocrystal-**II**, N···H contacts increase sharply from 5% in the analogue to 36.2%, suggesting significant intermolecular N–H interactions arising from the interaction between TCB and the analogue, which promotes charge-transfer (CT) interactions.

Table S5. Table for % interactions calculated using Hirshfeld surface analysis for the cocrystals of **1**.

Name	% Interactions													
	H··H	**O··H**	**N···H**	**C···H**	**C···C**	**C···N**	**C···O**	**C···F**	**H···F**	**N···N**	**N···F**	**O···F**	**F···F**	**O··O**
Cocrystal-I	23.8	6.9	1.3	10.5	9.1	0.4	2.2	7.9	31.0	0.2	1.1	1.9	3.4	0.1
Cocrystal-II	27.2	10.0	36.2	14.1	8.8	2.8	0.3	-	-	0.4	-	-	-	0.2
Cocrystal-III	33.5	15.3	3.0	10.6	3.6	-	1.5	3.7	23.3	-	2.0	1.5	1.8	0.2

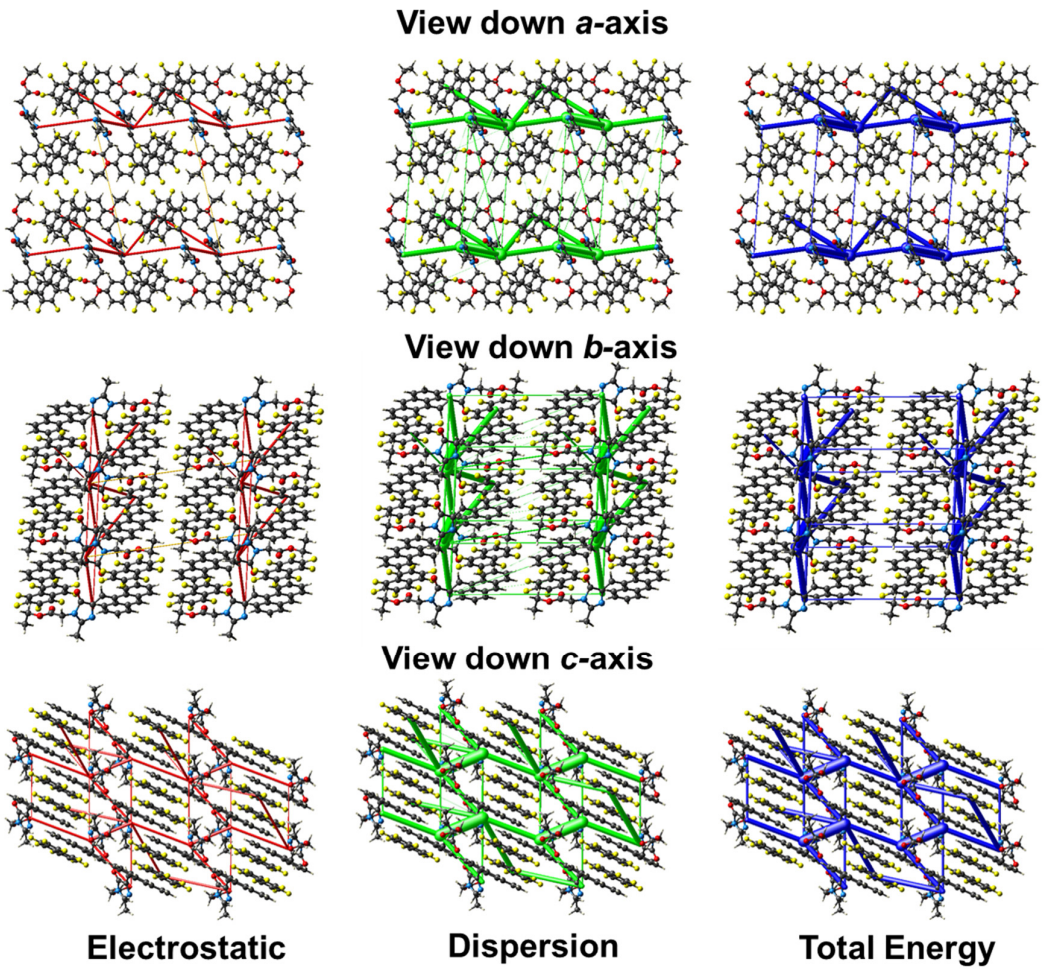

Figure S11. The energy frameworks for Cocrystal-**I**, showing the contributions of electrostatic and dispersion energies to the total energy (tube size = 100 and energy cut-off = 5 kJ/mol).

Table S6. Pairwise interaction energy based on energy frameworks for Cocrystal-**I**.

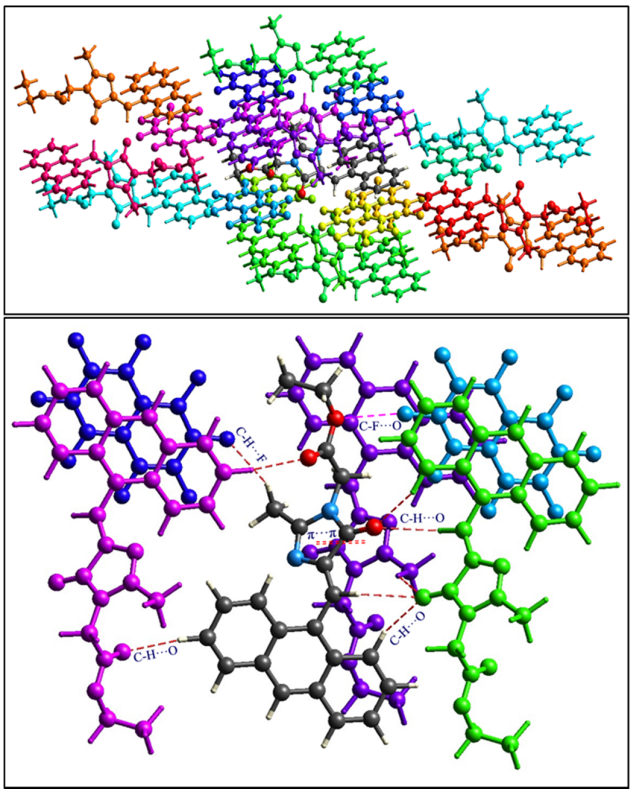

Interaction Energies (kJ/mol)
R is the distance between molecular centroids (mean atomic position) in Å.

Total energies, only reported for two benchmarked energy models, are the sum of the four energy components, scaled appropriately (see the scale factor table below)

	N	Symop	R	Electron Density	E_ele	E_pol	E_dis	E_rep	E_tot
	1	-x, -y, -z	16.53	B3LYP/6-31G(d,p)	0.3	-0.1	-3.9	0.0	-3.2
	2	x, y, z	17.87	B3LYP/6-31G(d,p)	-0.2	-0.1	-1.3	0.0	-1.4
	1	-	5.96	B3LYP/6-31G(d,p)	0.0	-0.9	0.0	0.0	-0.6
	1	-	10.32	B3LYP/6-31G(d,p)	0.5	nan	-1.3	0.0	nan
	1	-	6.34	B3LYP/6-31G(d,p)	2.0	-0.4	-4.1	0.0	-1.7
	1	-x, -y, -z	7.08	B3LYP/6-31G(d,p)	-17.8	-9.5	-36.3	36.0	-35.1
	2	x, y, z	7.51	B3LYP/6-31G(d,p)	-6.9	-2.4	-13.5	8.2	-15.7
	1	-	11.13	B3LYP/6-31G(d,p)	-0.3	-0.0	-1.0	0.0	-1.1
	2	x, y, z	15.58	B3LYP/6-31G(d,p)	-1.2	-0.7	-10.2	0.0	-10.6
	1	-	9.34	B3LYP/6-31G(d,p)	-17.8	-9.5	-36.3	36.0	-35.1
	1	-	6.06	B3LYP/6-31G(d,p)	-6.9	-2.4	-13.5	8.2	-15.7
	1	-	9.26	B3LYP/6-31G(d,p)	-16.6	-3.5	-43.3	39.3	-33.5
	1	-x, -y, -z	5.54	B3LYP/6-31G(d,p)	-23.3	-7.3	-97.8	61.6	-77.2
	1	-x, -y, -z	7.73	B3LYP/6-31G(d,p)	-16.6	-3.5	-43.3	39.3	-33.5
	1	-	13.61	B3LYP/6-31G(d,p)	-0.1	-0.1	-1.3	0.0	-1.3
	1	-x, -y, -z	17.70	B3LYP/6-31G(d,p)	4.8	-0.8	-10.7	0.0	-4.9

Scale factors for benchmarked energy models
See Mackenzie et al. IUCrJ (2017)

Energy Model	k_ele	k_pol	k_disp	k_rep
CE-HF ... HF/3-21G electron densities	1.019	0.651	0.901	0.811
CE-B3LYP ... B3LYP/6-31G(d,p) electron densities	1.057	0.740	0.871	0.618

In Cocrystal-**I**, the strongest interaction stabilizing the crystal structure is the π-π stacking interaction between two imidazolinone rings, with an energy of -77.2 kJ mol^{-1}. The second strongest interactions arise from C-H···O contacts, contributing -33.5 and -35.1 kJ mol^{-1} to lattice stabilization. Additionally, a C-F···O interaction between the analogue and the PFN coformer contributes -35.1 kJ mol^{-1}.

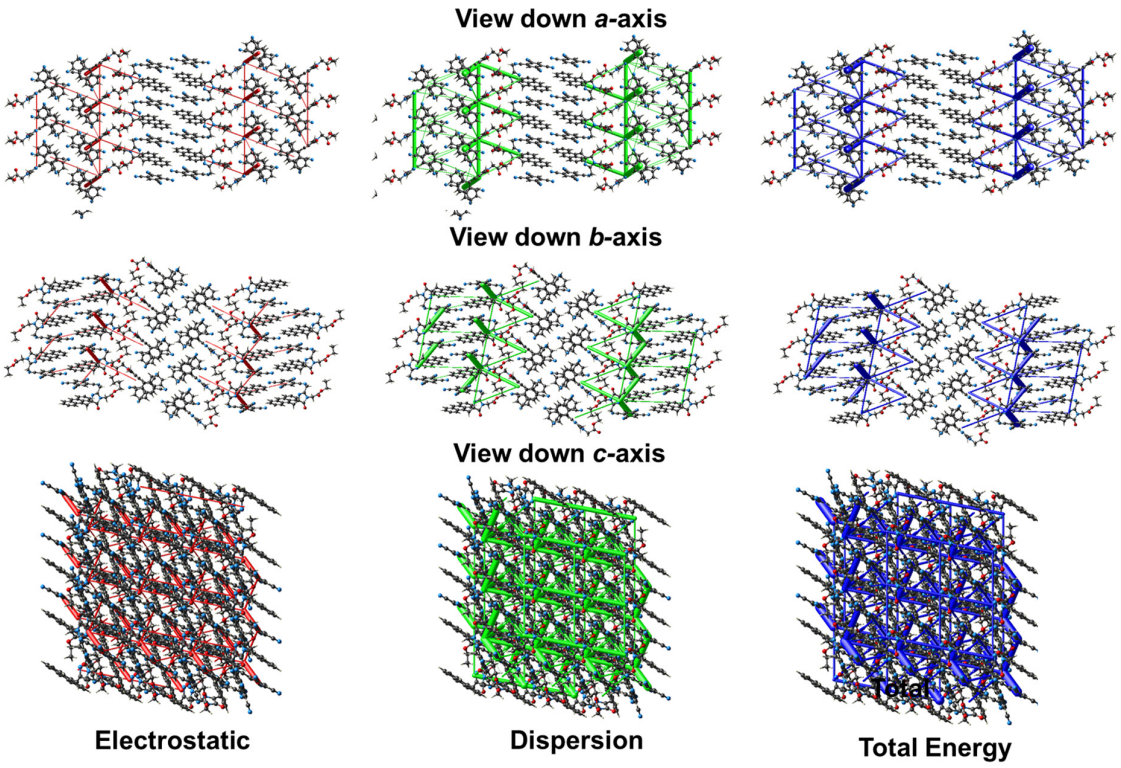

Figure S12. The energy frameworks for Cocrystal-**II** showing electrostatic and dispersion energy contributions to the total energy (tube size = 100 and energy cut-off = 5 KJ/mol).

Table S7. Pair wise interaction energy based on energy frameworks for Cocrystal-**II**.

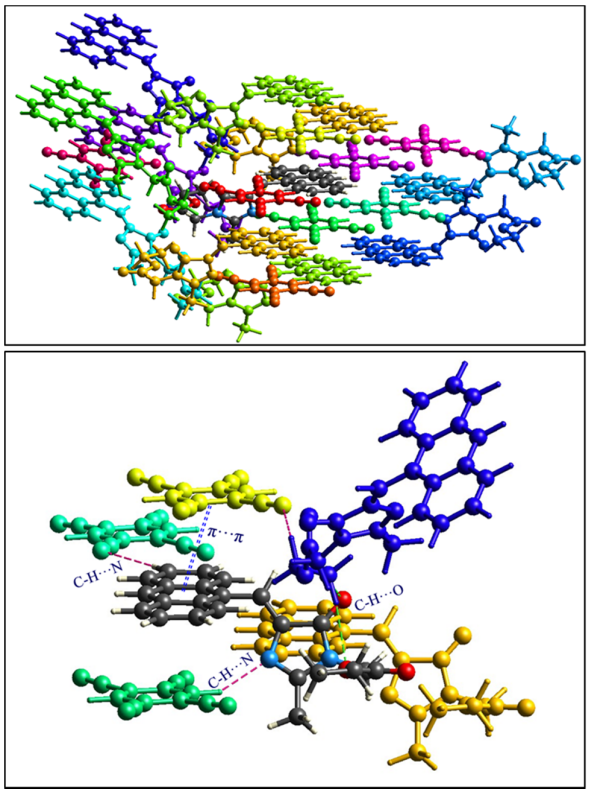

Interaction Energies (kJ/mol)
R is the distance between molecular centroids (mean atomic position) in Å.

Total energies, only reported for two benchmarked energy models, are the sum of the four energy components, scaled appropriately (see the scale factor table below)

N	Symop	R	Electron Density	E_ele	E_pol	E_dis	E_rep	E_tot
1	-	9.23	B3LYP/6-31G(d,p)	-1.3	0.0	-10.0	13.2	-1.8
1	-	7.19	B3LYP/6-31G(d,p)	-7.0	-3.0	-10.7	3.7	-16.7
2	x, y, z	7.84	B3LYP/6-31G(d,p)	-9.6	-0.8	-46.9	38.7	-27.7
1	-	5.57	B3LYP/6-31G(d,p)	-12.1	-1.7	-58.6	35.6	-43.2
2	x, y, z	8.01	B3LYP/6-31G(d,p)	-4.0	-3.9	-9.9	3.3	-13.7
1	-	10.33	B3LYP/6-31G(d,p)	0.0	-3.4	0.0	0.0	-2.5
1	-	4.64	B3LYP/6-31G(d,p)	0.0	-15.7	0.0	0.0	-11.6
1	-	12.30	B3LYP/6-31G(d,p)	-7.1	-0.9	-9.2	0.0	-16.1
1	-	9.51	B3LYP/6-31G(d,p)	-4.0	-1.9	-9.9	3.3	-12.2
1	-x, -y, -z	13.98	B3LYP/6-31G(d,p)	-1.0	-0.2	-6.7	0.0	-7.0
1	-x, -y, -z	13.67	B3LYP/6-31G(d,p)	1.1	-0.3	-8.2	0.0	-6.2
1	-	11.19	B3LYP/6-31G(d,p)	-9.6	-2.0	-46.9	38.7	-28.6
1	-	11.53	B3LYP/6-31G(d,p)	-1.2	-0.1	-1.0	0.0	-2.2
1	-	10.69	B3LYP/6-31G(d,p)	-1.8	-1.1	-6.4	5.5	-4.9
1	-	11.34	B3LYP/6-31G(d,p)	1.2	-0.0	-6.6	2.1	-3.2
1	-	12.24	B3LYP/6-31G(d,p)	0.0	-3.5	0.0	0.0	-2.6

Scale factors for benchmarked energy models
See Mackenzie et al. IUCrJ (2017)

Energy Model	k_ele	k_pol	k_disp	k_rep
CE-HF ... HF/3-21G electron densities	1.019	0.651	0.901	0.811
CE-B3LYP ... B3LYP/6-31G(d,p) electron densities	1.057	0.740	0.871	0.618

In Cocrystal-**II**, strong π-π interactions between the analogue and the coformer, as well as C-H···π stacking between the C-H of the anthracene interacts with the imidazolinone ring, contributing significantly to lattice stabilization, with interaction energies of -43.2 and -27.7 kJ mol^{-1}, respectively. C-H···O interactions between the analogue molecules, as well as a pair of N-H···N interactions between the analogue and the coformer, also contribute, with lattice interaction energies of -28.6, -11.6, and -16.1 kJ mol^{-1}, respectively.

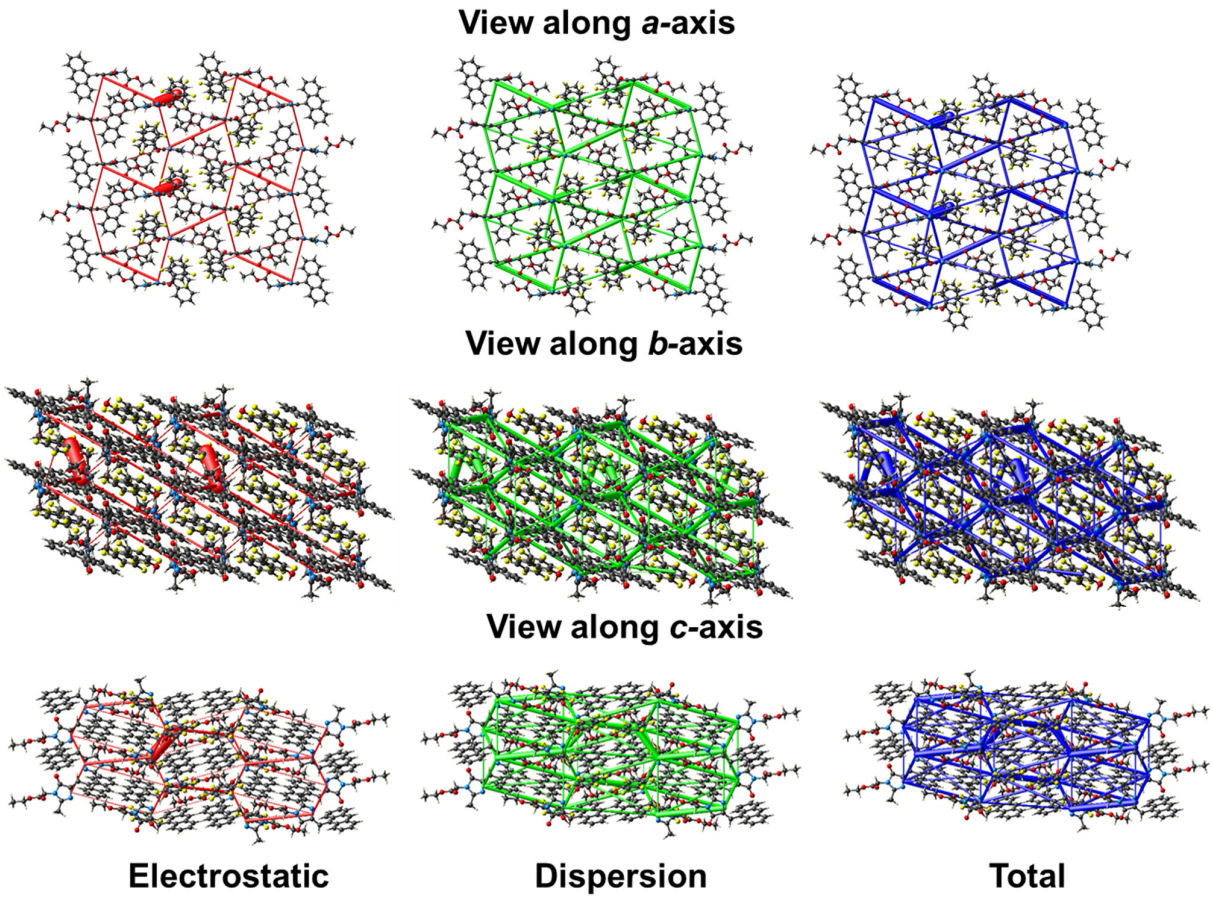

Figure S13. The energy frameworks for Cocrystal-**III** show electrostatic and dispersion energy contributions to the total energy (tube size = 100 and energy cut-off = 5 KJ/mol).

Table S8. Pairwise interaction energy based on energy frameworks for Cocrystal-**III**.

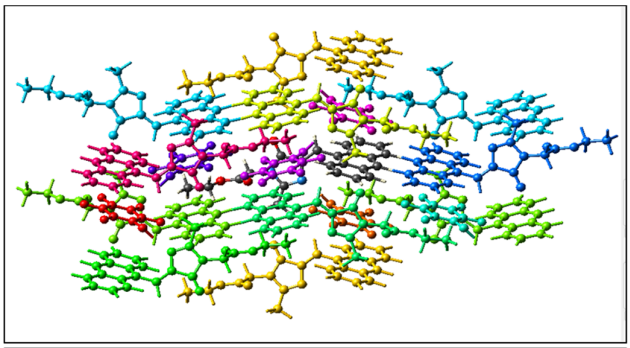

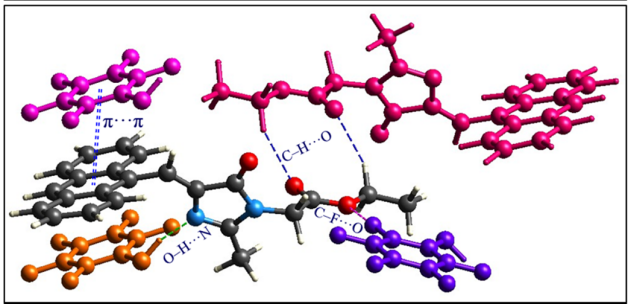

Interaction Energies (kJ/mol)
R is the distance between molecular centroids (mean atomic position) in Å.

Total energies, only reported for two benchmarked energy models, are the sum of the four energy components, scaled appropriately (see the scale factor table below)

N	Symop	R	Electron Density	E_ele	E_pol	E_dis	E_rep	E_tot
1	-	13.33	B3LYP/6-31G(d,p)	-1.1	-0.2	-5.9	0.0	-6.5
1	-	5.16	B3LYP/6-31G(d,p)	-83.1	-2.0	-53.4	110.9	-67.4
2	x, y, z	7.74	B3LYP/6-31G(d,p)	-3.9	-2.0	-11.6	9.7	-9.7
2	x+1/2, -y+1/2, z+1/2	8.22	B3LYP/6-31G(d,p)	-1.1	-7.0	-11.2	5.0	-13.0
2	-x+1/2, y+1/2, -z+1/2	11.81	B3LYP/6-31G(d,p)	-4.9	-1.9	-30.3	16.6	-22.8
1	-x, -y, -z	12.76	B3LYP/6-31G(d,p)	-4.4	-0.6	-6.1	0.0	-10.4
2	x+1/2, -y+1/2, z+1/2	8.58	B3LYP/6-31G(d,p)	-11.6	nan	-25.2	25.6	nan
1	-	10.31	B3LYP/6-31G(d,p)	-2.9	-0.2	-7.8	7.9	-5.1
2	-x+1/2, y+1/2, -z+1/2	12.28	B3LYP/6-31G(d,p)	-3.4	-1.9	-17.0	0.0	-19.8
1	-x, -y, -z	13.05	B3LYP/6-31G(d,p)	2.6	-0.5	-18.0	0.0	-13.3
1	-	6.07	B3LYP/6-31G(d,p)	-3.4	-0.8	-22.5	8.8	-18.3
1	-	9.18	B3LYP/6-31G(d,p)	-0.7	-0.6	-12.7	6.7	-8.1
1	-	8.95	B3LYP/6-31G(d,p)	-0.6	-0.1	-2.4	0.1	-2.7
1	-	5.13	B3LYP/6-31G(d,p)	-5.7	-1.3	-52.4	25.6	-36.8
1	-x, -y, -z	10.40	B3LYP/6-31G(d,p)	-19.9	-3.4	-47.1	32.3	-44.6

Scale factors for benchmarked energy models
See Mackenzie et al. IUCrJ (2017)

Energy Model	k_ele	k_pol	k_disp	k_rep
CE-HF ... HF/3-21G electron densities	1.019	0.651	0.901	0.811
CE-B3LYP ... B3LYP/6-31G(d,p) electron densities	1.057	0.740	0.871	0.618

In Cocrystal-**III**, the strongest interaction is the O-H···N hydrogen bond, with an interaction energy of -67.4 kJ mol^{-1}, followed by a C-H···O interaction with an energy of -44.6 kJ mol^{-1}. Additionally, π···π interactions between the analogue and the coformer and C-F···O contacts contribute -36.8 and -8.1 kJ mol^{-1}, respectively, to the total lattice energy.

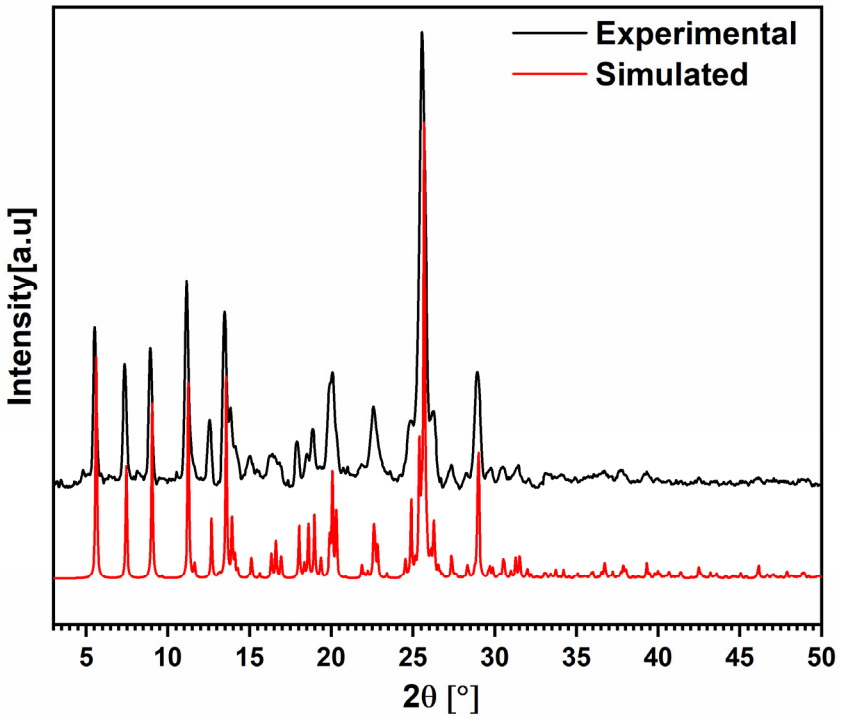

Figure S14. Overlay of experimental and calculated PXRD pattern of Cocrystal-**I**.

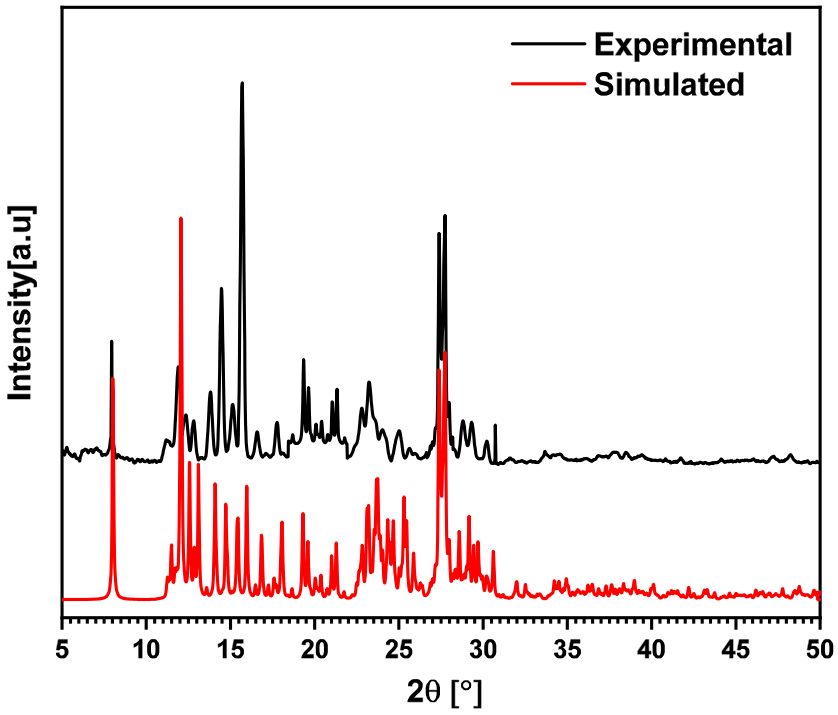

Figure S15. Overlay of experimental and calculated PXRD pattern of Cocrystal-**II**.

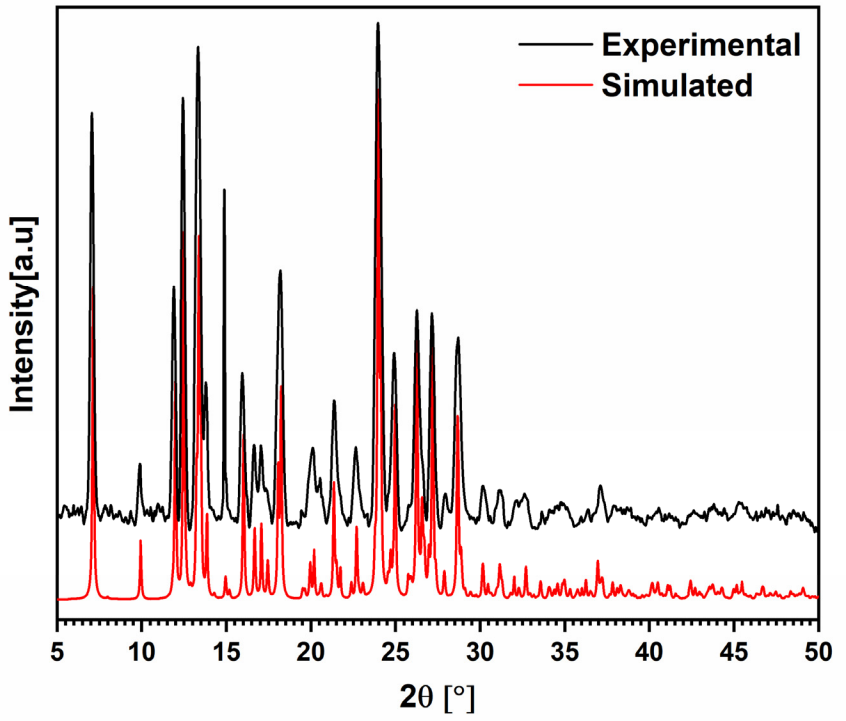

Figure S16. Overlay of experimental and calculated PXRD pattern of Cocrystal-**III**.

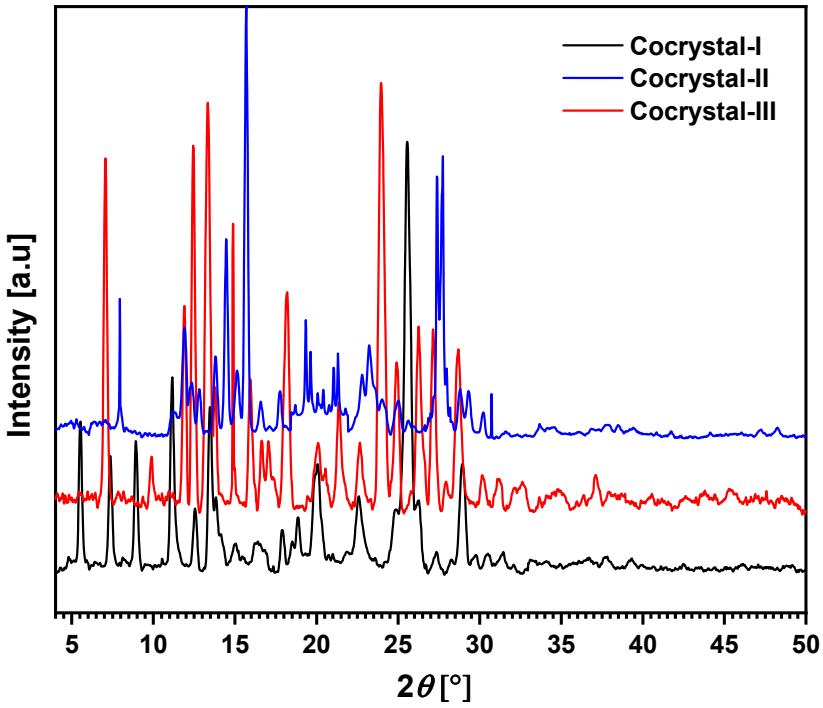

Figure S17. Overlay of experimental PXRD patterns of all the cocrystals of **1**.

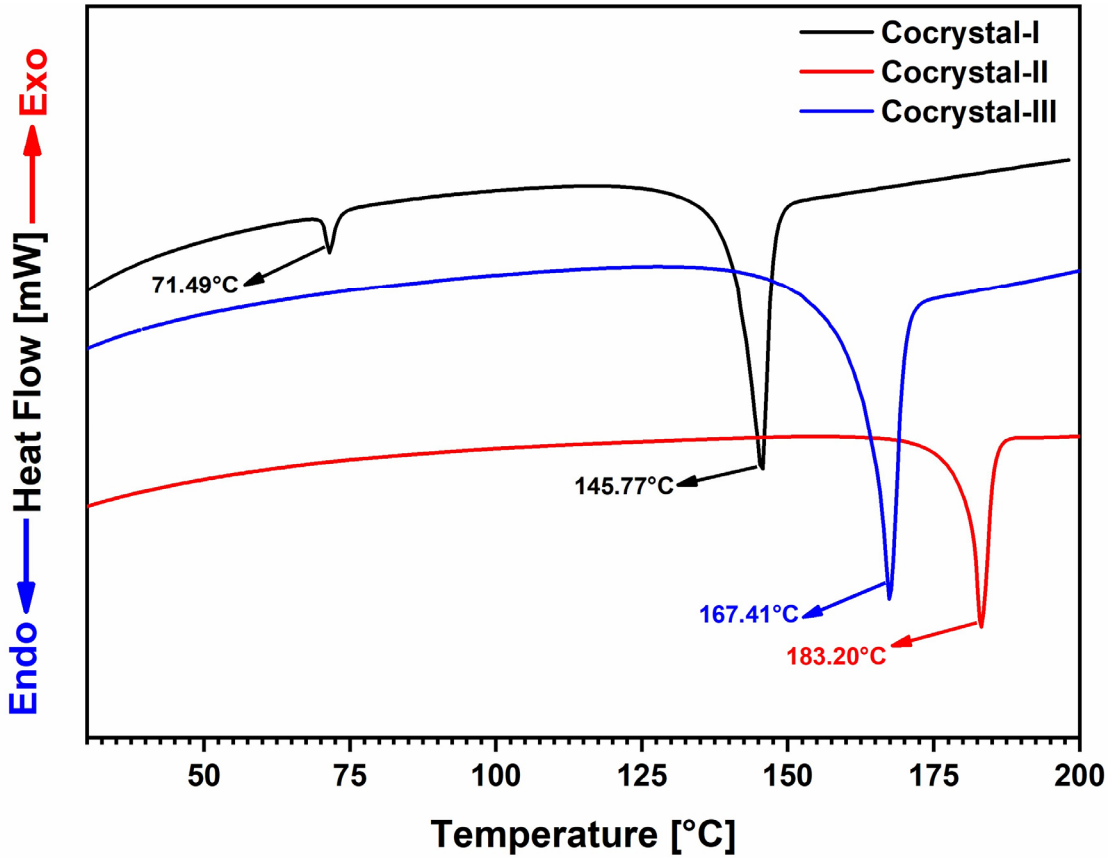

Figure S18. Overlay of DSC thermograms of all the cocrystals of **1**.

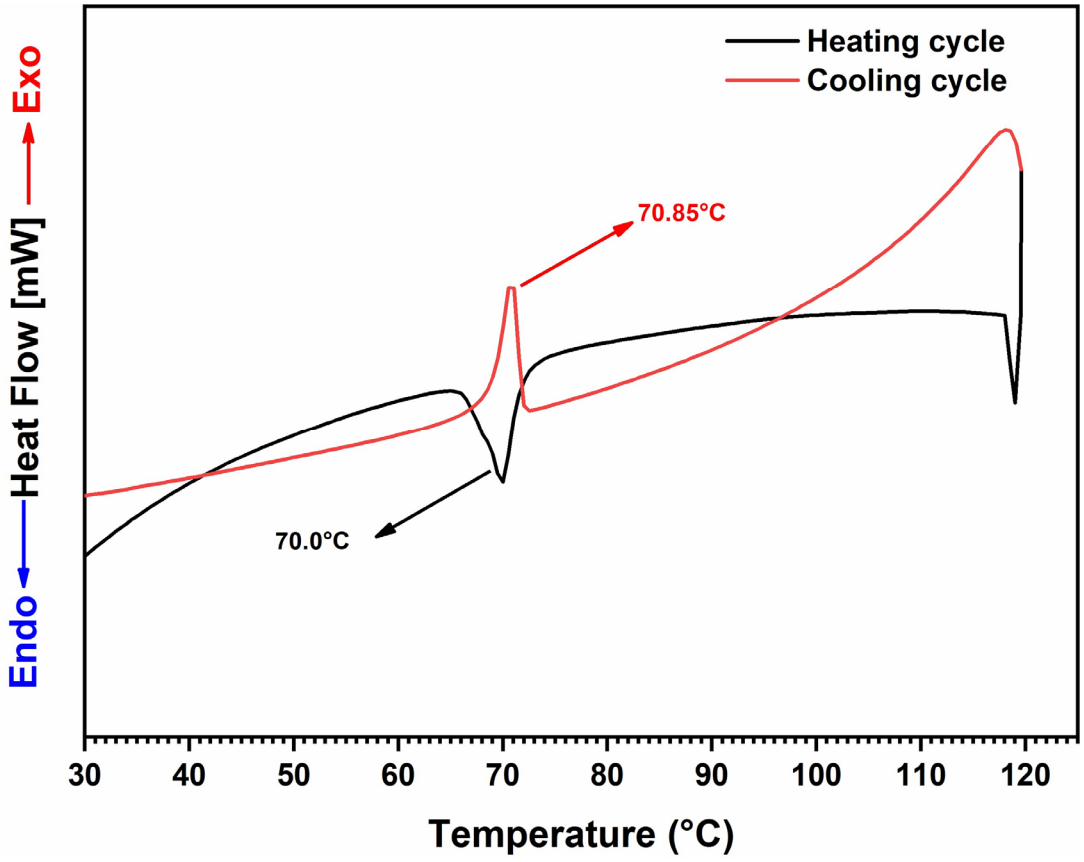

Figure S19. DSC thermogram of Cocrystal-**I** showing a reversible phase transition between Cocrystal-**I** and Cocrystal-**IA**.

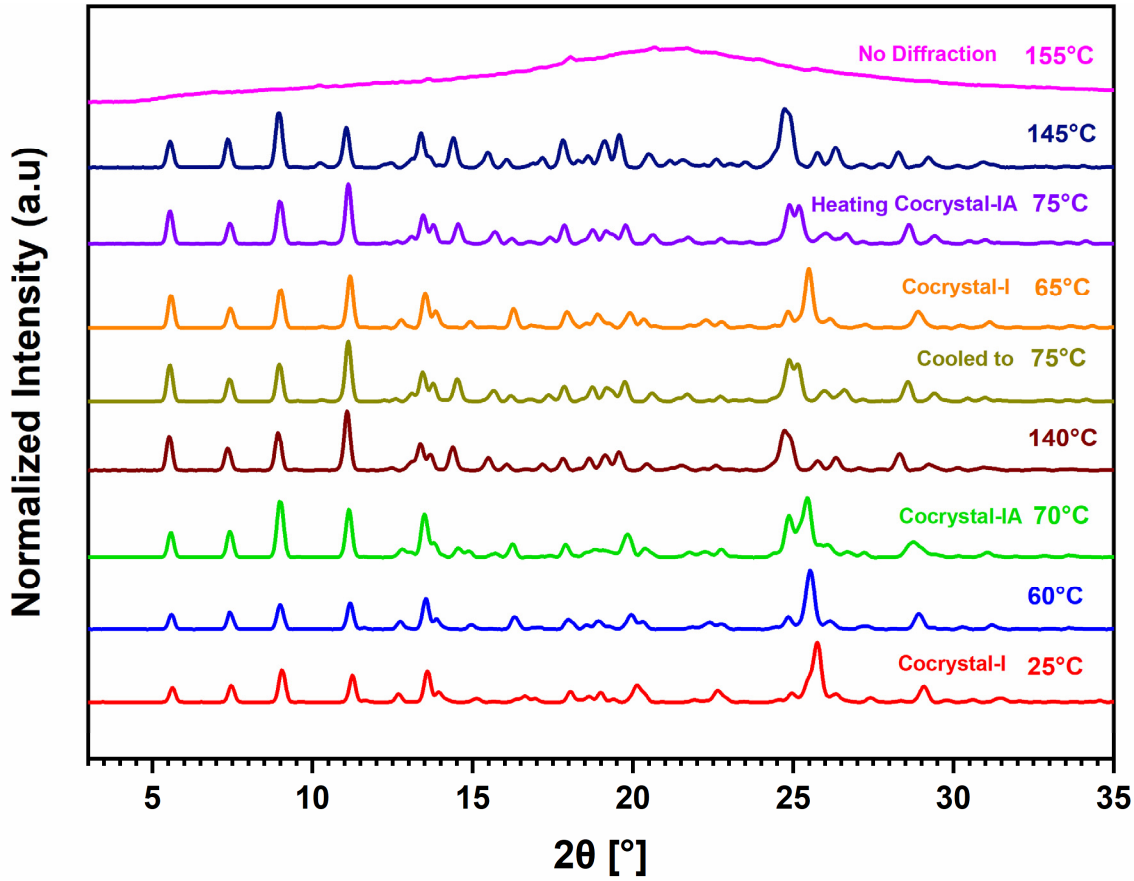

Figure S20. VT-PXRD profiles for Cocrystal-**I** recorded at different temperatures.

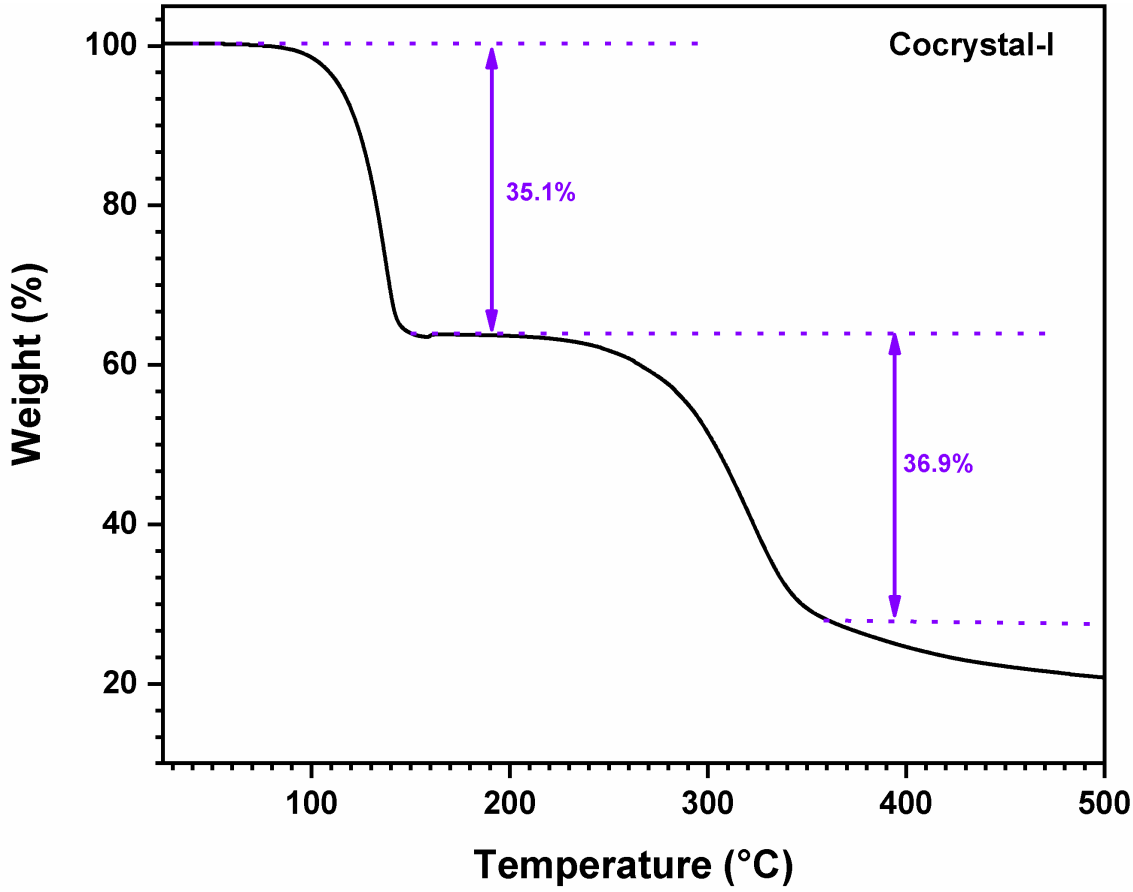

Figure S21. Thermogravimetric analysis (TGA) thermogram of Cocrystal-**I**.

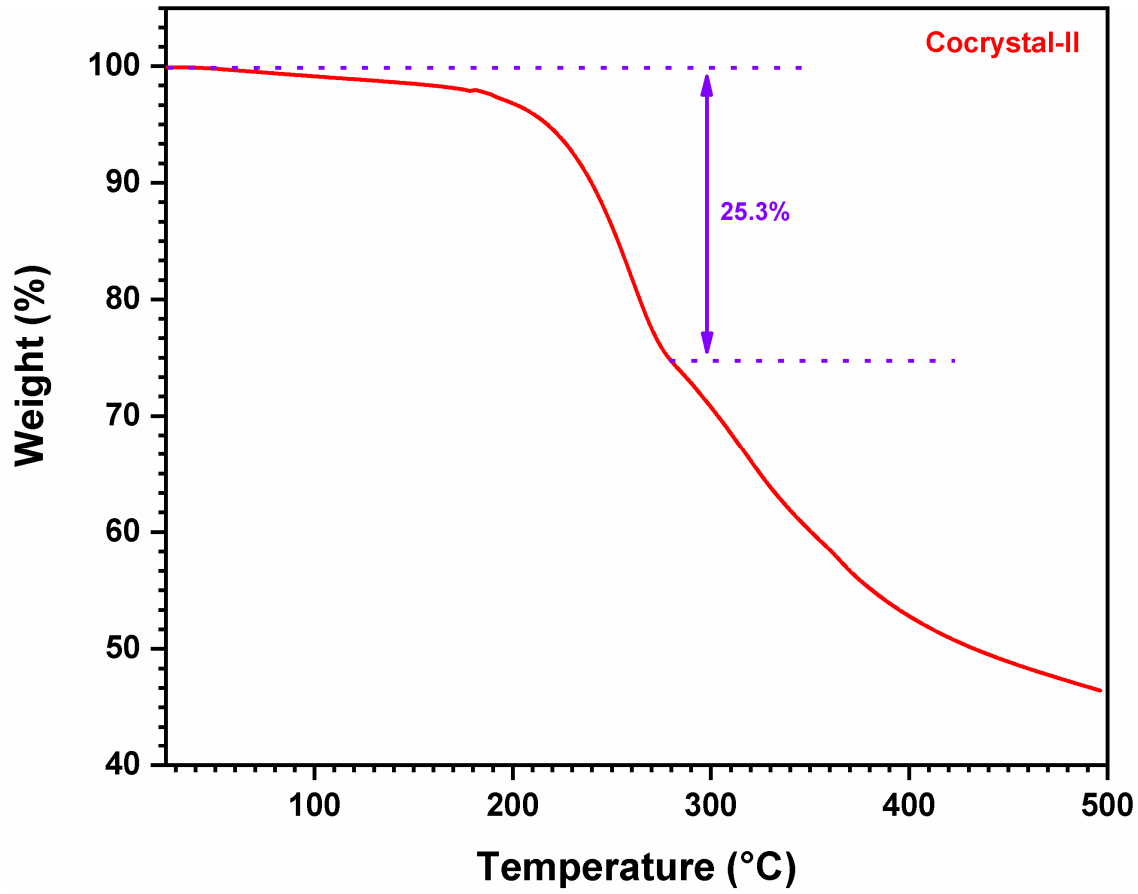

Figure S22. Thermogravimetric analysis (TGA) thermogram of Cocrystal-**II**.

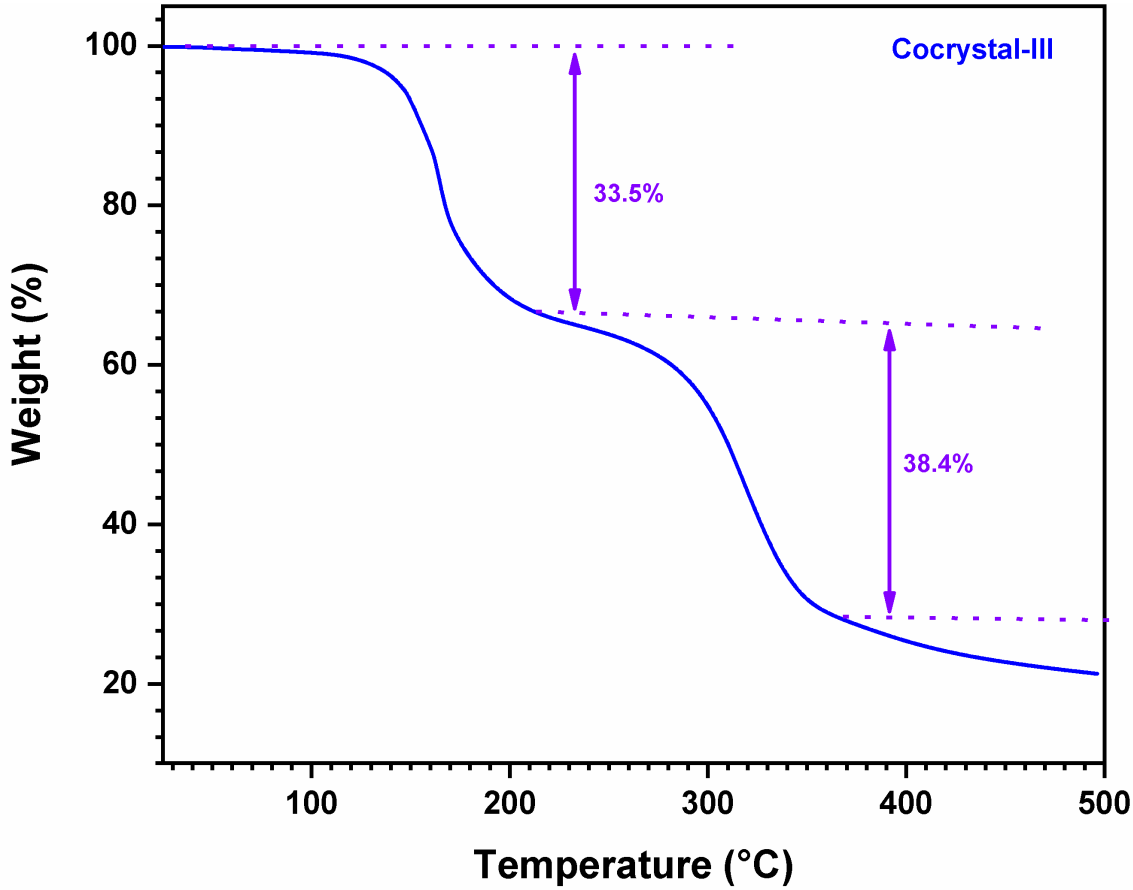

Figure S23. Thermogravimetric analysis (TGA) thermogram of Cocrystal-**III**.

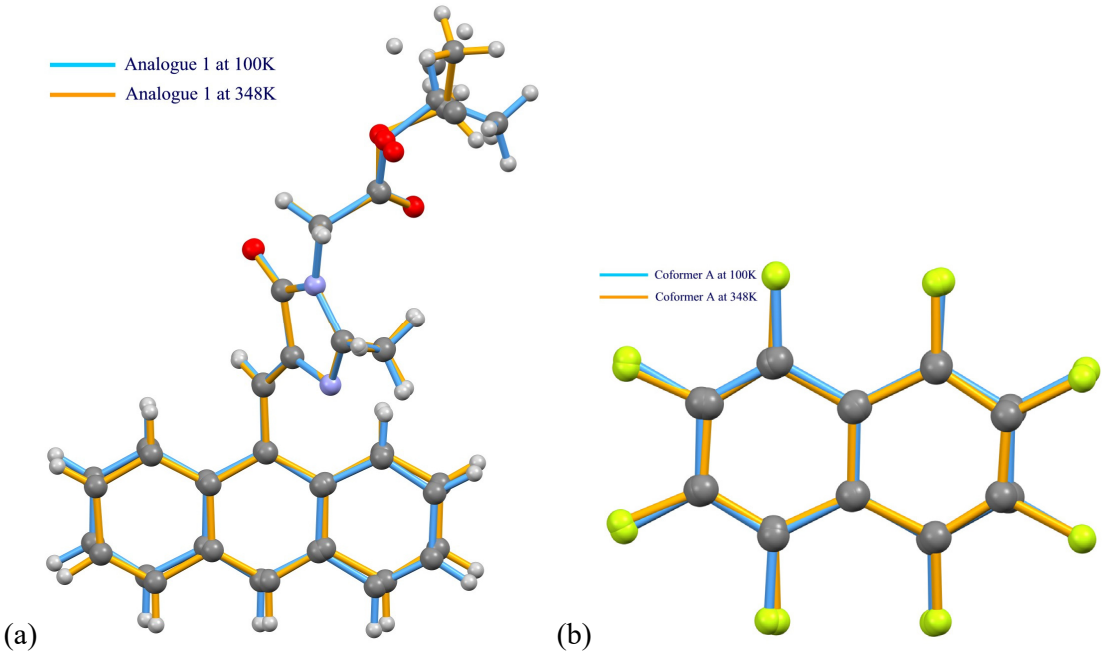

(a) (b)

Figure S24. Overlay of the crystal structures of conformers of (a) **1** and (b) PFN in Cocrystal-**I** and Cocrystal-**IA**.

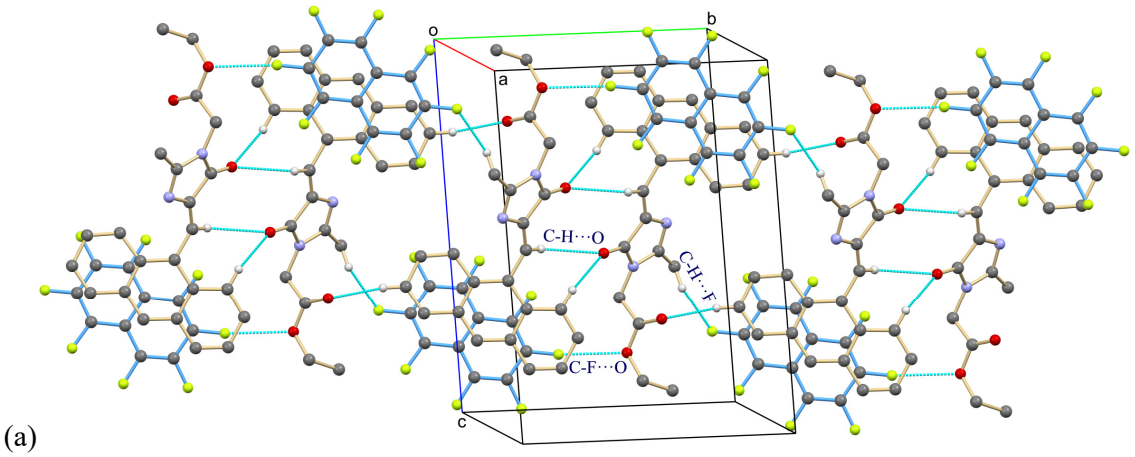

(a)

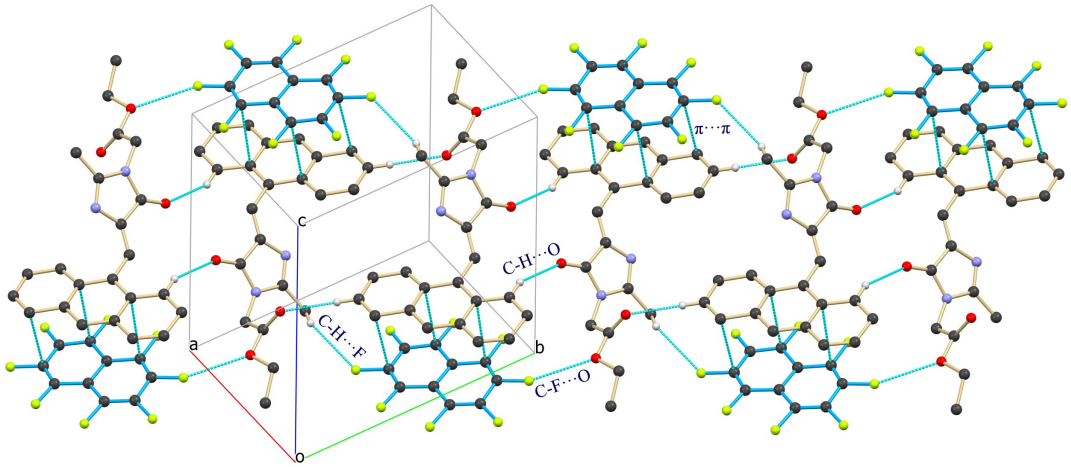

(b)

Figure S25. Molecular packing in the Cocrystal-**I** (a) and **IA** (b), showing similarity with the formation of 1D molecular string parallel to the *b*-axis using C-H···O, C-H···F and C-F···O interactions.

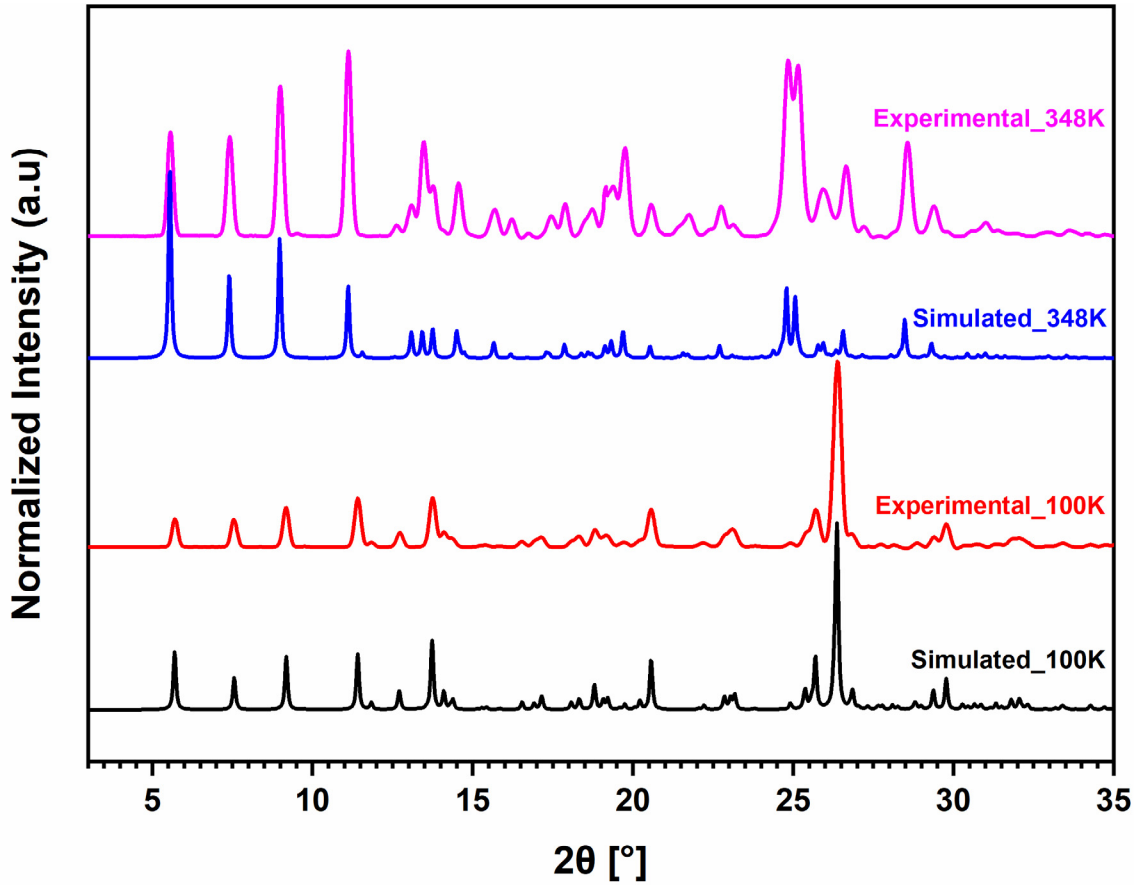

Figure S26. Overlay of experimental and calculated PXRD patterns of Cocrystal-**I** (black and red) and Cocrystal-**IA** (blue and pink).

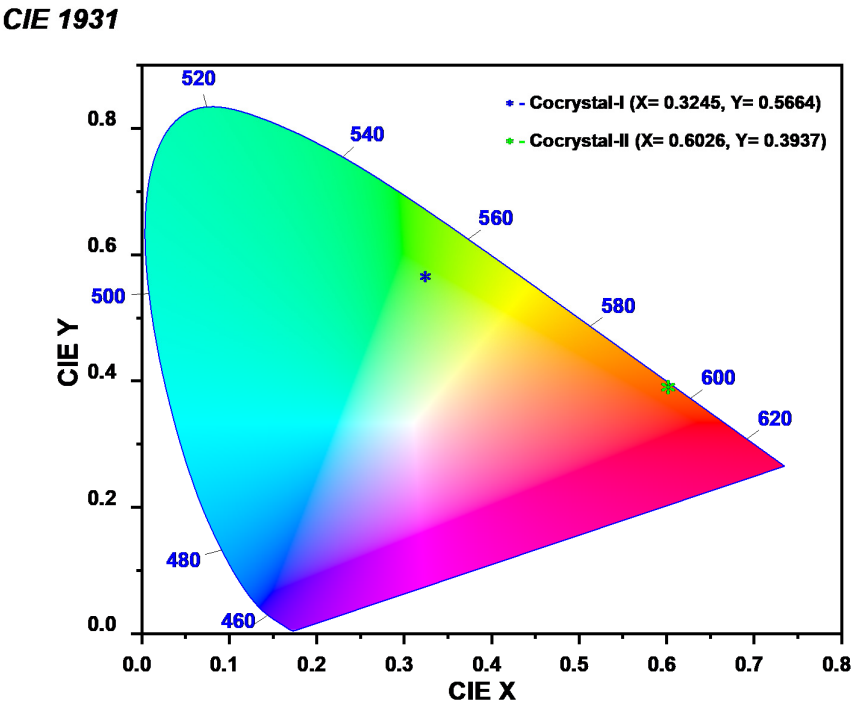

Figure S27. The CIE coordinates position on chromaticity for Cocrystal-**I** (blue star), and Cocrystal-**II** (green star) in the crystalline state.

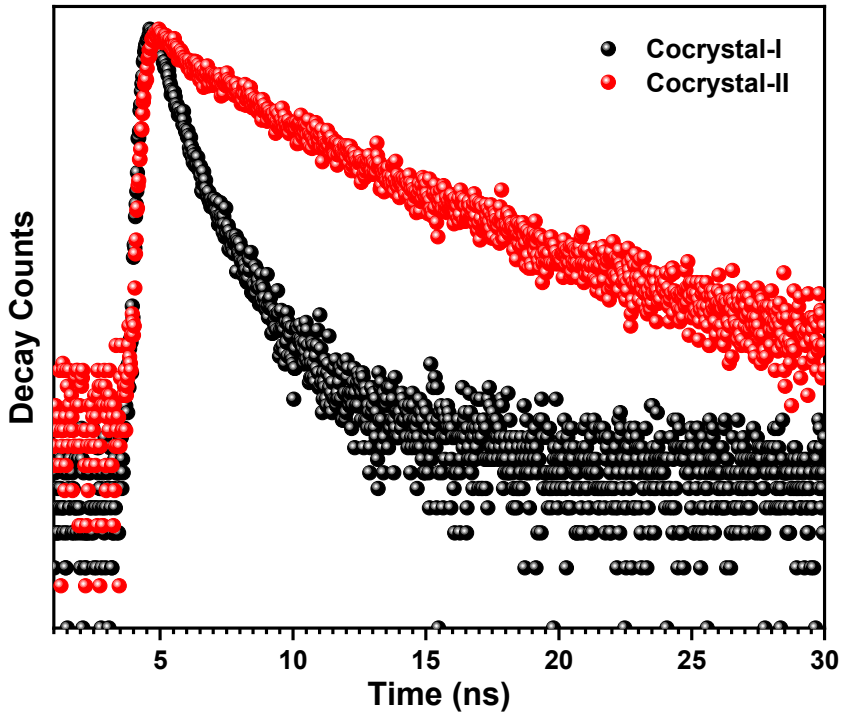

Figure S28. Room temperature time-resolved PL decay curves for Cocrystal-**I** and Cocrystal-**II** of **1**.

Table S9. Emission maxima, emission quantum yield (%), and fluorescence lifetime measurement for all the cocrystals of **1** in the solid-state, (ND- not detectable).

Cocrystals	**λ_{em} [nm]**	**Φ_f (%)**	**τ_1 [ns]**	**τ_2 [ns]**	**Relative (%)**		**τ_{ave}[ns]**	**K_r ($10^7 s^{-1}$)**	**K_{nr} ($10^8 s^{-1}$)**
					a1	a2			
Cocrystal-I	509	3.45	1.04	5.16	81.90	18.10	3.19	1.08	3.03
Cocrystal-II	631	6.3	2.88	7.84	26.82	73.18	7.25	0.87	1.29
Cocrystal-III	ND	ND	ND	ND	ND	ND	ND	ND	ND

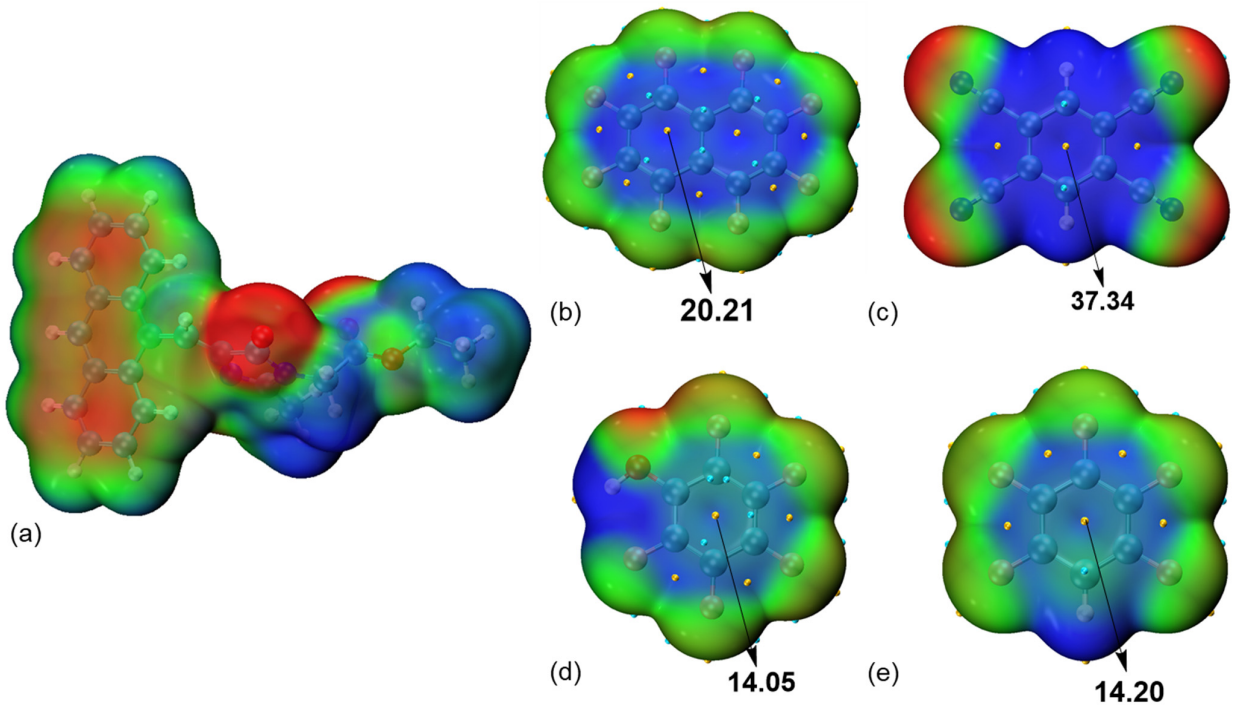

Figure S29. Calculated electrostatic potential (ESP) distribution maps for (a) GFPc analogue **1**, (b-d) coformer molecules A-C, and (e) pentafluorobenzene; with their respective maxima (Vs, max in kcal/mol). Blue and red represent the positive and negative regions, respectively, while green denotes the intermediate zone between them. The isovalue of the isodensity surface is set at 0.001 a.u.

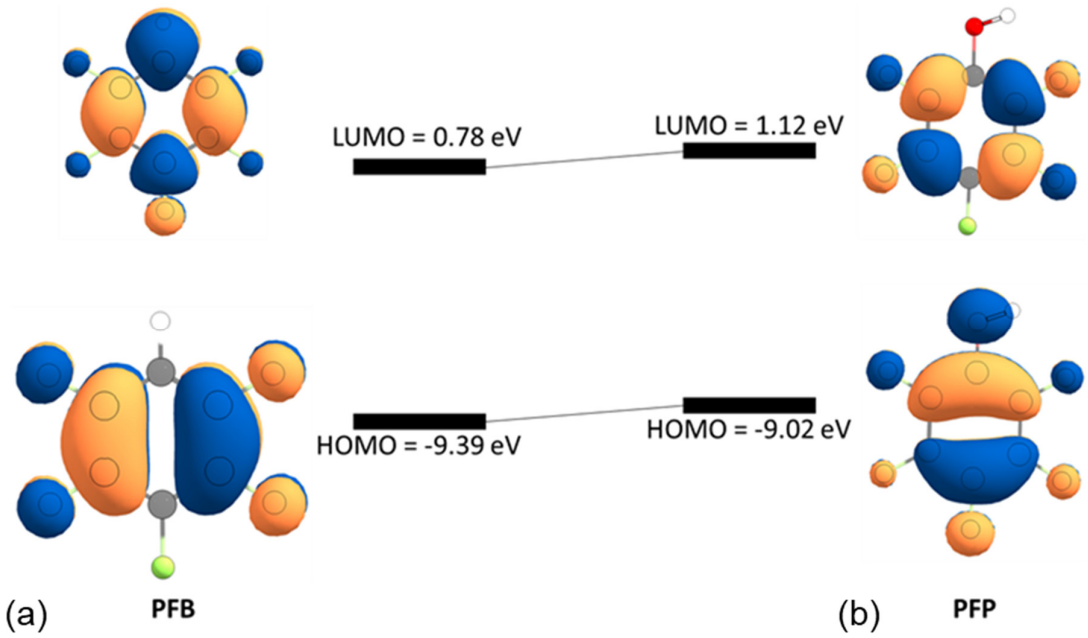

Figure S30. Molecular orbitals and their corresponding energy levels for (a) PFB and (b) PFP.

The impact of hydrogen positions and structural relaxation on the ground-state electron density prior to excited-state calculations was explicitly assessed. Hydrogen atoms in the experimental crystal structures were first corrected to neutron-standard bond lengths following established crystallographic practice. Subsequently, a constrained ground-state DFT optimization was carried out in which only hydrogen atoms were allowed to relax, while all heavy atoms were kept fixed at their experimentally determined positions to preserve the solid-state packing. To directly evaluate whether hydrogen relaxation affects the ground-state wavefunction relevant for excited-state properties, we performed ground-state electron density difference (EDD) analysis by subtracting the electron density of the H-corrected experimental structure from that of the constrained H-optimized structure using identical real-space grids. The resulting EDD maps (Figure S31) show that electron density redistribution is strictly localized around H-atoms, corresponding to minor local reshaping of the σ density. Importantly, no significant density redistribution is observed over the π-conjugated chromophore backbone or intermolecular contact regions, which are most relevant for the photophysical behavior discussed in this work. This analysis demonstrates that hydrogen relaxation does not alter the topology or character of the ground-state wavefunction associated with the chromophore and validates the use of experimentally derived geometries for subsequent TD-DFT analysis. On this basis, the conclusions drawn from the original TD-DFT calculations remain robust.

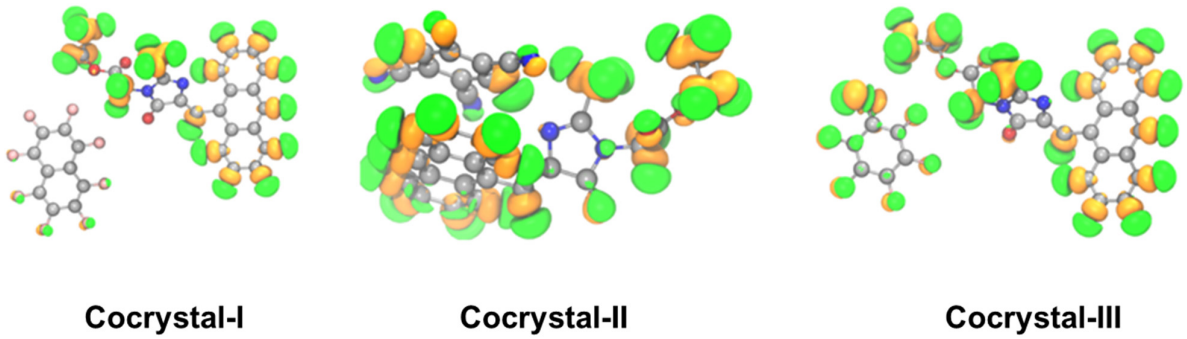

Figure S31. Ground-state electron density difference (EDD) maps for the three cocrystals, obtained by subtracting the electron density of the H-corrected experimental structures from that of the constrained H-optimized geometries. Green (+0.003 au) and yellow (−0.003 au) isosurfaces represent electron density accumulation and depletion, respectively. In all cases, density redistribution is localized around hydrogen atoms, with negligible perturbation of the π-conjugated framework and intermolecular interaction regions.

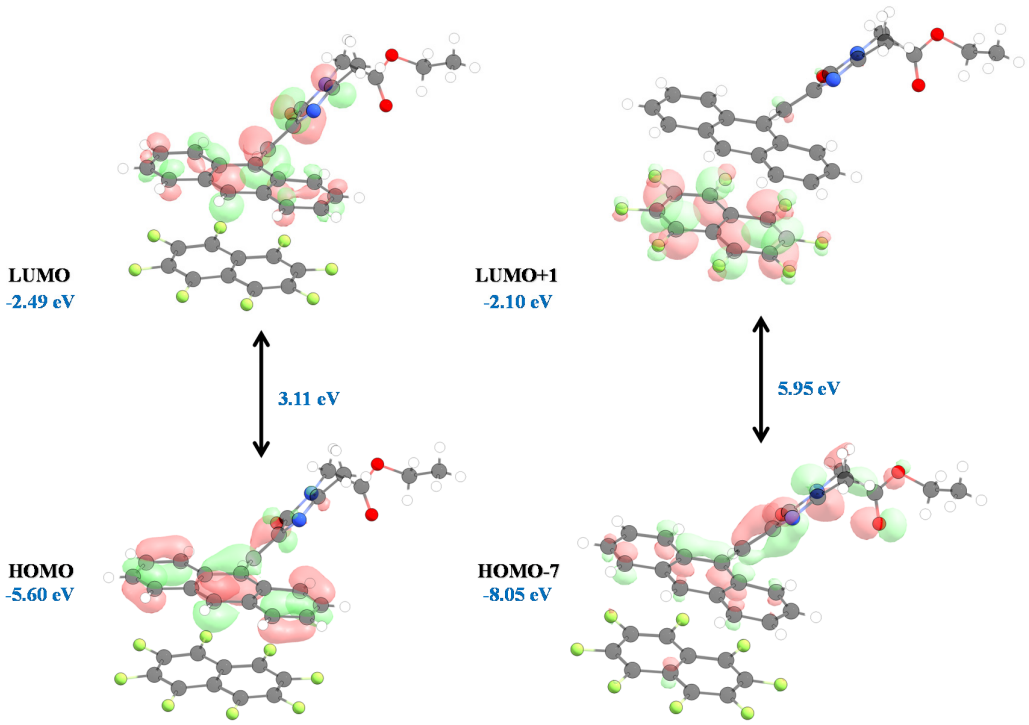

Figure S32. Molecular orbitals and their corresponding energy levels for Cocrystal-**I** calculated using the Gaussian 09 program by employing the B3LYP/6-311++g(d,p) level of theory.

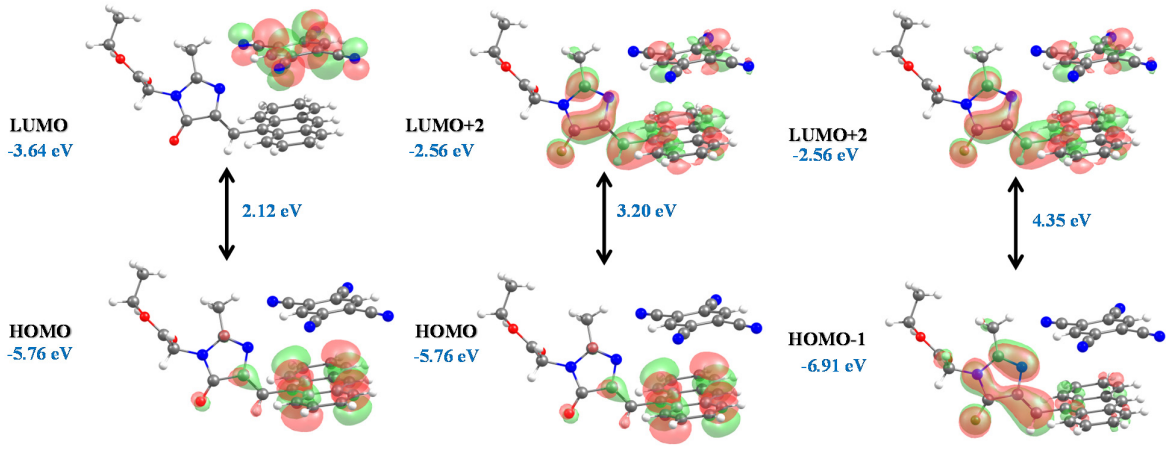

Figure S33. Molecular orbitals and their corresponding energy levels for Cocrystal-**II** calculated using the Gaussian 09 program by employing the B3LYP/6-311++g(d,p) level of theory.

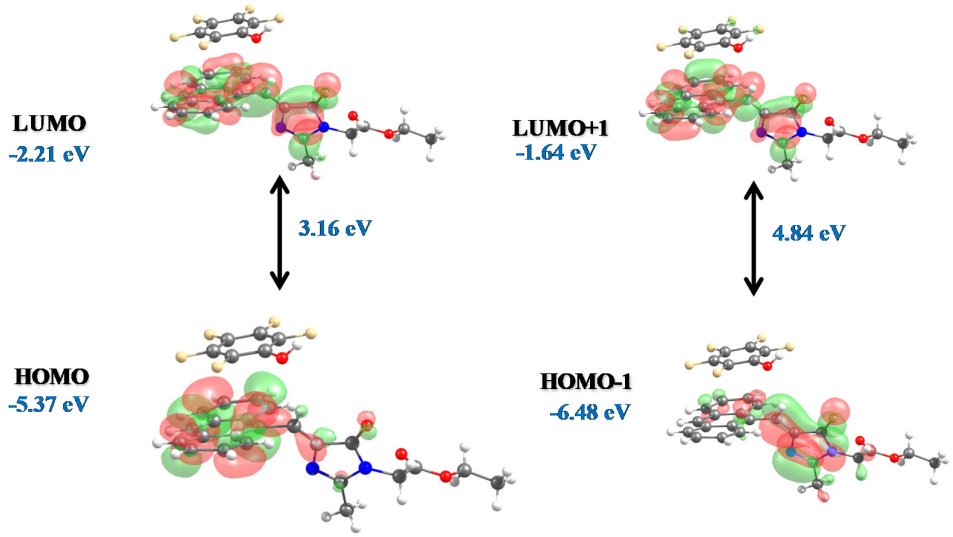

Figure S34. Molecular orbitals and their corresponding energy levels for Cocrystal-**III** calculated using the Gaussian 09 program by employing the B3LYP/6-311++g(d,p) level of theory.

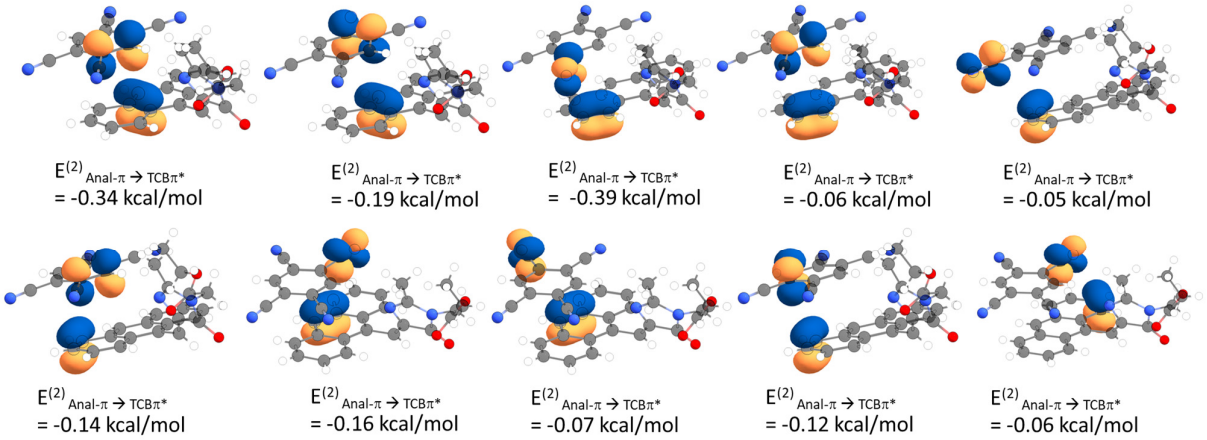

Figure S35. Natural bond orbital (NBO) analysis for Cocrystal-**II**, calculated by employing the ωB97X-D/def2-TZVP level of theory.

Calculations of Photophysical Parameters:

The photophysical parametres were calculated using following equations from references 16-18:

1. $\tau_{ave} = a_1 (\tau_1)^2 + a_2 (\tau_2)^2 / a_1 \tau_1 + a_2 \tau_2$
2. $K_r = \Phi_F / \tau_F$
3. $K_{nr} = (1/\tau_F) - Kr$

where,

K_r=Radiative rate constant of fluorescence

K_{nr}=Non-radiative rate constant of fluorescence

Φ_F=Fluorescence quantum yield

τ_F= Fluorescence lifetime

Bandgap calculations:

The bandgap calculation is carried out by the following Davis-Mott relation (tau-plot),

$\alpha h\nu = A (h\nu - Eg)^n$

Where,

A = energy independent constant

Eg = Optical energy gap

α = Absorption coefficient

n - Denotes the nature of transition

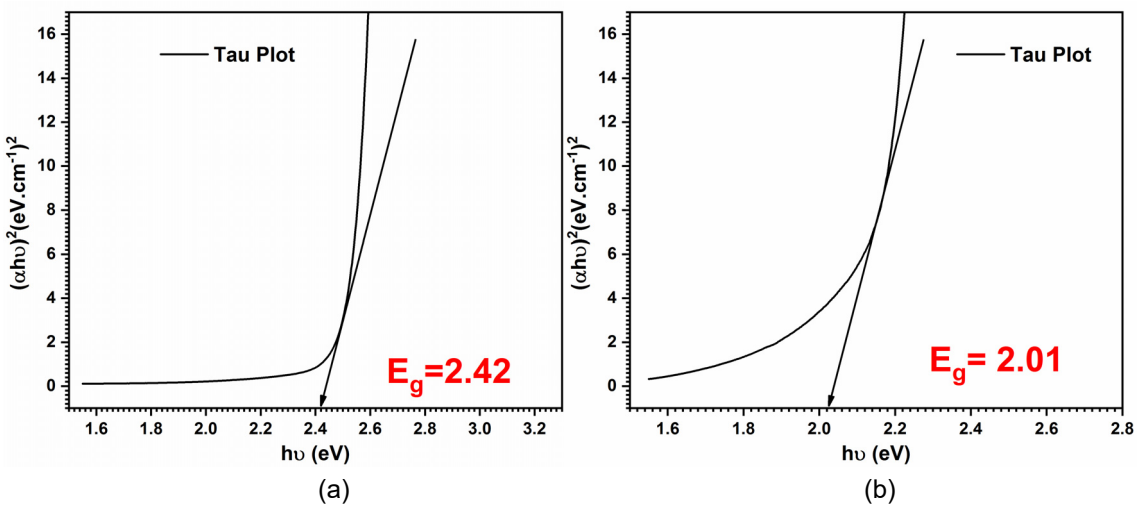

Figure S36. Tauc plot of UV-visible absorption data for the calculation of band gap energy for (a) Cocrystal-**I**, and (b) Cocrystal-**II**.

Table S10. Bandgap, transition values and degree of ionicity (ρ) calculated for all the cocrystals of **1** (f = oscillator strength).

Cocrystal	**Experimental Tau plot (eV)**	**TD-DFT [B3LYP/6-311G++(d,p)]**		**The degree of ionicity (ρ)**	
		Transition (eV/nm)	**Involved Orbitals**	**Mulliken charge analysis**	**NBO charge analysis**
Cocrystal-**I**	2.42	457.99 nm 2.7071 eV HOMO → LUMO f=0.1783	252.75 nm 4.9053 eV HOMO-7 → LUMO+1 f=0.2613	0.028	0.00526
Cocrystal-**II**	2.01	460.79 nm 2.6907 eV HOMO → LUMO+2 f=0.1045	319.13 nm 3.8851 eV HOMO-1 → LUMO+2 f=0.0920	0.056	0.02709
Cocrystal-**III**	-	463.45 nm 2.6752 eV HOMO → LUMO f=0.1218	289.88 nm 4.2771 eV HOMO-1 → LUMO+1 f=0.0845	0.015	0.00203

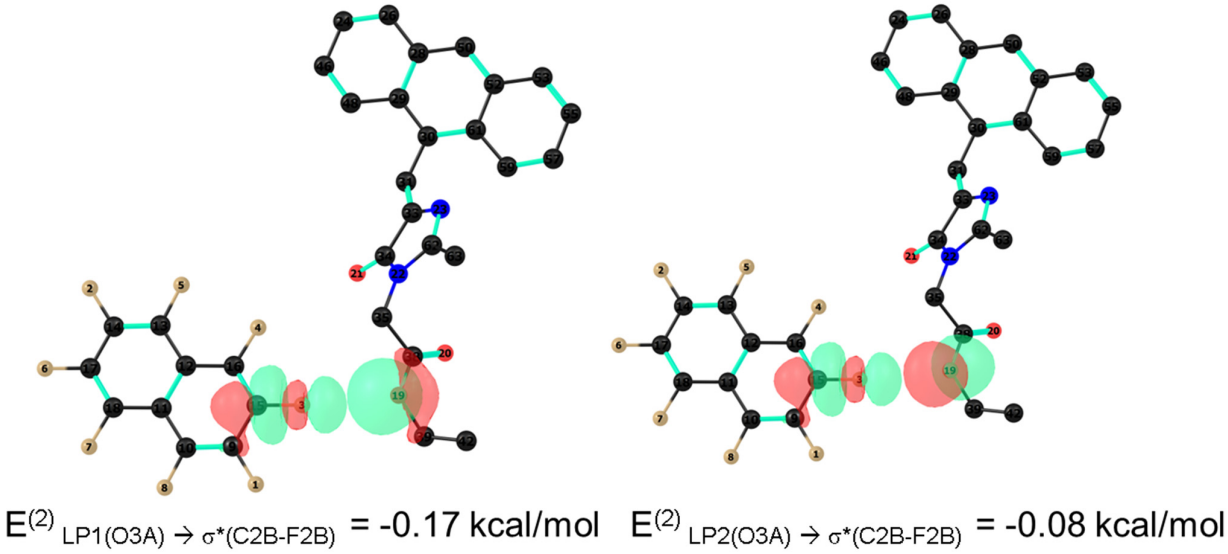

Figure S37. Natural bond orbital (NBO) analysis for Cocrystal-**I**, calculated by employing the ωB97X-D/def2-TZVP level of theory.

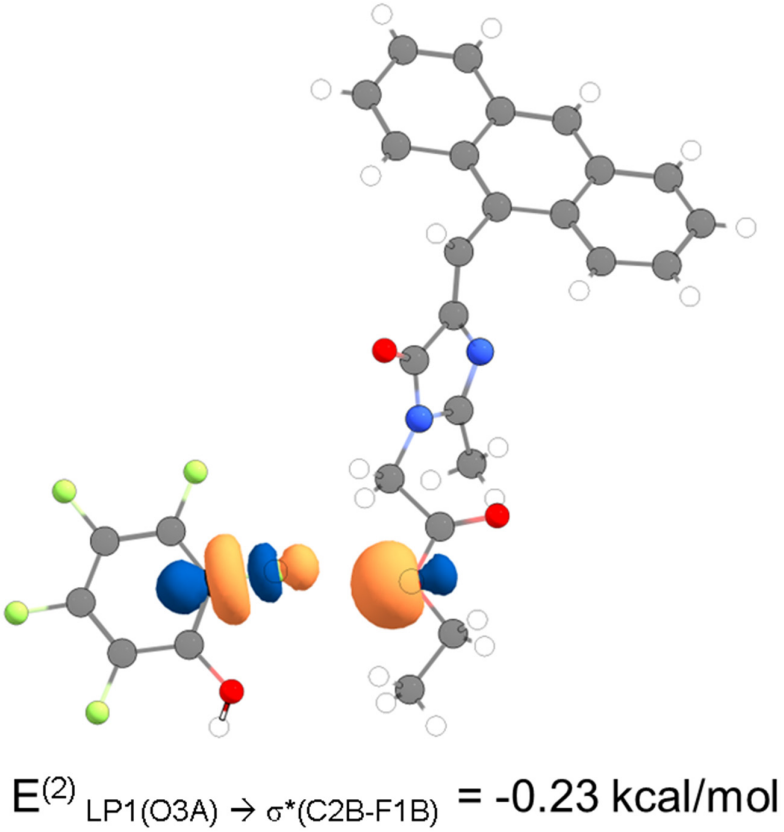

Figure S38. Natural bond orbital (NBO) analysis for Cocrystal-**III**, calculated by employing the ωB97X-D/def2-TZVP level of theory.

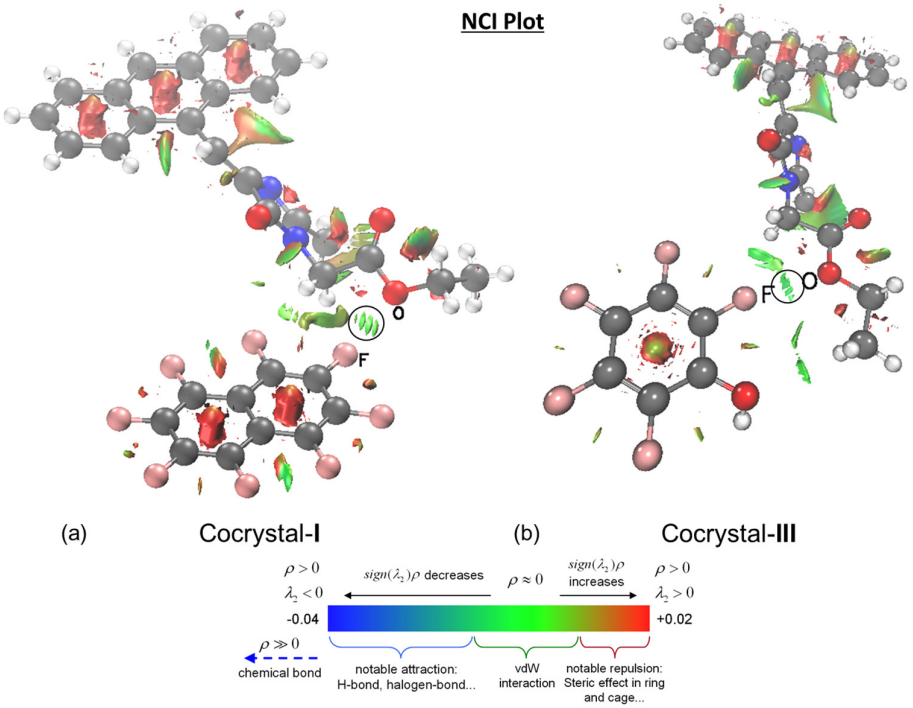

Figure S39. Noncovalent interaction (NCI) plots for (a) Cocrystal-**I**, and (b) Cocrystal-**III**.

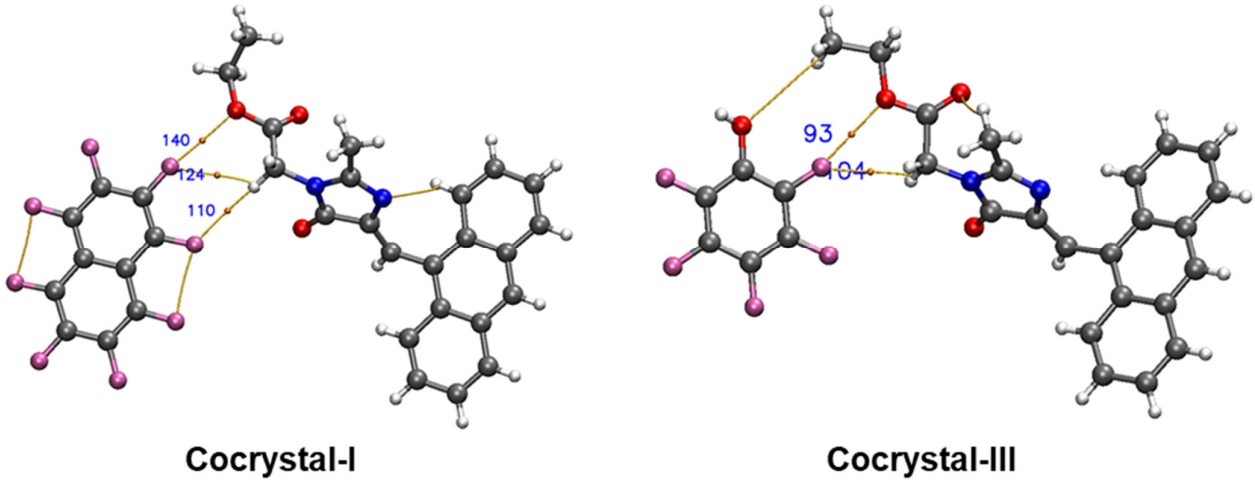

Figure S40. Quantum theory for atom in molecule (QTAIM) analysis for Cocrystal-**I**, and Cocrystal-**III**.

Table S11. Electron density descriptors such as total electron density ρ(r), Laplacian of the electron density $\nabla^2\rho(r)$, Hamiltonian kinetic energy K(r), Lagrangian kinetic energy G(r), potential energy density V(r), energy density H(r), and electron localization function (ELF) at desired BCP for Cocrystal-**I** and Cocrystal-**III** are shown here.

System	BCP	ρ(r)	$\nabla^2\rho(r)$	G(r)	V(r)	H(r)	G(r)/ρ(r)	ELF
Cocrystal-I	F---O (140)	0.0072	0.0409	0.0076	-0.0051	0.0025	1.05	0.0102
	F---H (124)	0.0033	0.015	0.0029	-0.0019	0.0009	0.87	0.0055
	F---H (110)	0.0036	0.015	0.0029	-0.002	0.0009	0.80	0.0071
Cocrystal-III	F---O (93)	0.0076	0.0431	0.0081	-0.0055	0.0026	1.06	0.0108
	F---H (104)	0.0046	0.023	0.0043	-0.0029	0.0014	0.93	0.0071

References:

1 Bruker. APEX3, SAINT-Plus and SADABS; Bruker AXS Inc: Madison, Wisconsin, USA, 2016.

2 G. M.Sheldrick, *Acta Crystallogr. Sect. A Found. Crystallogr.,* 2008, **64**, 112–122.

3 G. M. Sheldrick, *Acta Crystallogr. Sect. C Struct. Chem.,* 2015, **C71**, 3–8.

4 C. F. Macrae, I. Sovago, S. J.Cottrell, P. T. A. Galek, P. McCabe, E. Pidcock, M.Platings, G. P. Shields, J. S. Stevens, M. Towler and P. A. Wood, *J. Appl. Cryst.,* 2020, **53**, 226−235.

5 A. L. Spek, *J. Appl. Cryst.,* 2003, **36**, 7–13.

6 P. R. Spackman, M. J. Turner, J. J. McKinnon, S. K. Wolff, D. J. Grimwood, D. Jayatilaka and M. A. Spackman, *J. Appl. Cryst.,* 2021, **54**, 1006–1011.

7 M. A. Spackman and D. Jayatilaka, *CrystEngComm*, 2009, **11**, 19-32.

8 M. A. Spackman and J. J. McKinnon, *CrystEngComm*, 2002, **4**, 378–392.

9 M. J. Turner, S. P. Thomas, M. W. Shi, D. Jayatilaka and M. A. Spackman, *Chem. Comm.*, 2014, **51**, 3735–3738.

10 O'Neill, *Powder Diffraction*, 2013, **28**, 137–148.

11 A. D. Becke, *J. Chem. Phys.*, 1993, **98**, 5648–5652.

12 T. Lu and F. Chen, *J. Comput. Chem.,* 2011, **33,** 580–592.

13 W. Humphrey, A. Dalke and K. Schulten, *J. Mol. Graph.*, 1996, **14**, 33–38.

14 J.-D. Chai, *Phys. Chem. Chem. Phys.*, 2008, **10**, 6615.

15 F. Weigend and R. Ahlrichs, *Phys. Chem. Chem. Phys.*, 2005, **7**, 3297.

16 J. R. Lakowicz, Principles of Fluorescence Spectroscopy, *Springer*, New York, 2006, DOI: 10.1007/978-0-387-46312-4.

17 B. R. Kaafarani, T. H. El-Assaad, W. A. Smith, S. M. Ryno, F. Hermerschmidt, J. Lyons, D. Patra, B. Wex, E. J. W. List-Kratochvil, C. Risko, S. Barlow and S. R. Marder, *J. Mater. Chem. C*, 2019, **7**, 5009–5018.

18 J. Tauc, R. Grigorovici and A. Vancu, *Phys. Status Solidi B*, 1966, **15**, 627–637.